Computer Networks 185 (2021) 107672

Contents lists available at ScienceDirect

Computer Networks

journal homepage: www.elsevier.com/locate/comnet

Performance analysis of coverage-centric heterogeneous cellular networks using dual-slope path loss model

Khurram Shehzad [*,a], Noor M Khan [a], Junaid Ahmed [b]

[a] ACME Center for Research in Wireless Communications (ARWiC), Department of Electrical Engineering, Capital University of Science and Technology, Islamabad, Pakistan

[b] Department of Electrical and Computer Engineering, COMSATS University Islamabad, Pakistan

ARTICLE INFO

Keywords:
Coverage probability
Dual-slope path loss model
Interference management
Load balancing
Non-uniform heterogeneous cellular networks
Stochastic geometry

ABSTRACT

Densifying the cellular networks has been largely considered as a promising solution in meeting the capacity demands of emerging cellular networks that have expeditiously transformed from voice-oriented to data-oriented. However, densifying the network infrastructure is like a double-edged sword; it on one hand helps in achieving the desired data rates but on the other hand, it degrades the network coverage. Owing to the disparity in transmit power of macro base stations (MBSs) and small BSs (SBSs), the SBSs located in the close proximity of MBSs have negligible coverage areas that not only overburden the macro tier but also cause excessive interference. In order to overcome these limitations, we propose to mute the SBSs that are located in the near-vicinity of MBSs to introduce a partial-correlation between the locations of the BS tiers. Meanwhile, to further enhance the coverage performance of these coverage-centric cellular networks, the traditional load balancing mechanism along with interference abating strategy is also employed in this paper. Nonetheless, it is also well-known in the literature that the usage of single-slope path loss model (PLM) leads to significant inaccuracies in evaluating the performance of dense cellular networks. Therefore, a more accurate PLM based on the dual-slope is adopted in this paper. Analytical expressions for the tier association and coverage probability are derived for a randomly chosen user using the tools from stochastic geometry and validated through simulations. The numerical results testify the improvement in network coverage due to the non-uniform deployment of SBSs and the joint consideration of load balancing and interference mitigation mechanisms.

1. Introduction

The past decade has witnessed an exponential increase in mobile data traffic, owing primarily to the drastic rise in the demand for high-end devices that support numerous high data rate applications. According to the mobility report published by Ericsson in 2019, the mobile data traffic is predicted to reach a mammoth 131 exabytes/month by year 2024, wherein the video traffic alone is expected to account for a significant 74% of the total traffic [1]. Interestingly, the cellular networks were originally designed for voice-oriented applications, but with the popularity of high-tech devices, the trend has clearly shifted towards data-hungry applications like high-definition video conferencing, telehealth, mobile television, interactive gaming, augmented/virtual reality and many others [2]. Hence, this two-pronged growth requires substantial increase not only in the peak data rates (bps) but also in data rate density (bps/km^2).

To accommodate such high data rate demands, the cellular network planners are considering densification of base stations (BSs) through proliferation of low-powered small BSs (SBSs) that vary in transmitting power, data rate, backhaul capacity, and/or physical size. Such combination of high and low powered BSs constitutes the heterogeneous cellular networks (HCNs) [3]. With the assistance of SBSs, the low coverage areas associated with macro BSs (MBSs) can be eliminated and the capacity can be improved in hot-spots [4]. In addition to these lucrative offerings, the deployment of SBSs alongside MBSs introduces new challenges that have to be addressed on the fly due to their dynamic nature. For instance, the capacity and coverage planning, effective utilization of radio and energy resources, subtle association strategies of user equipments (UEs) with BS tiers, management of interference etc [5,6].

From the perspective of modeling the locations of BSs and UEs, it is commonly accepted in the literature that the locations of UEs are

* Corresponding author.
E-mail address: engr.ksm@gmail.com (K. Shehzad).

https://doi.org/10.1016/j.comnet.2020.107672
Received 21 June 2020; Received in revised form 24 October 2020; Accepted 30 October 2020
Available online 2 November 2020

random, while the locations of BSs are relatively fixed and regular. However, with the dense deployment of SBSs in the overlaid network, the randomness associated with the BS positions is also rapidly increasing. Consequently, this increased randomness in the location of BSs necessitates adopting more tractable network modeling strategies that can circumvent the limitations of traditional approaches (Wyner and regular grid-based models). The authors in [7,8] have shown that the BS locations in both the conventional (single-tier) and multi-tier cellular networks can be precisely modeled by the point process models, e.g., PPP. The coverage area of the deployed cellular network in these models is generally obtained through the usage of Poisson-Voronoi tessellation (PVT) method. Nevertheless, it is pertinent to mention that the impact of environment on the propagation of signals has not been considered in the PVT based model, and hence smooth cellular coverage boundaries are obtained through it. Contrarily, in practical cellular networks, signals experience the anisotropic nature of the path loss fading and as a result, the cellular coverage boundaries are extremely irregular shaped [9–11].

Cellular networks are developing from voice-oriented to always available and uninterrupted mobile broadband data networks. Deploying densified SBSs in support of MBSs has been one of the primary driving forces in meeting the ever increasing capacity demands of emerging wireless networks [12]. The addition of these SBSs in the overlaid network is like a *double-edged sword*. Densifying the cellular networks brings the network resource in the close proximity of UEs but the excessive interference also has a detrimental impact on the performance of HCNs and it has been thoroughly addressed in numerous research works like [13–18]. In addition to interference management issues, the disparity in transmitting power of BS tiers is the root cause of load imbalance between BS tiers, which overburdens the macro tier and degrades the network performance as well. Load balancing in multi-tier cellular networks has also been studied extensively and various techniques have been employed to tackle it amicably [19–23].

2. Related works

Owing to the analytical tractability, all the BS tiers in an HCN are generally assumed to be randomly deployed in a service area. This simplistic strategy of no correlation between the location of BSs does not assist in increasing the network coverage by densifying BSs. This is because, the UEs associated with macro tier receive excessive interference from their nearby SBSs (especially the subscriber owned femto BSs), while the UEs which are offloaded to small BS tiers using SBS biasing face excessive interference from MBSs due to their higher transmit power [24]. Moreover, it is also a common assumption to consider a fully-loaded system i.e., all BSs are assumed to be always transmitting and serving their respective UEs [8,25]. The MBSs are generally known to have large coverage areas and hence, this assumption is valid for them. However, it is not true for the SBSs and as result, it leads to a pessimistic network coverage estimation. Therefore, it is important to consider the impact of BS loading especially given the density of BSs is quickly approaching the density of user devices. It has been shown in numerous research works [26–30] that the network coverage improves if the activity factor of low-powered BS tiers is assumed to be lesser than 1 i.e., all the SBSs are not active at all the times.

A two-tier HCN is shown in Fig. 1 which clearly shows that the coverage region of any SBS is sensitive to its distance from the neighboring MBSs. The SBSs which are located in near-vicinity of MBSs have very small coverage areas, while those located at the far distances from MBSs have reasonable coverage areas [31]. Besides this, it is also evident that a moderate level of SBS biasing would not be helpful in increasing the coverage areas of those SBSs which are in close proximity of MBSs. These observations clearly suggest that densifying SBSs without taking into consideration the distance from neighboring MBSs would not lead to improvement in the network coverage, and hence it highlights the need for exploring selective or non-uniform densification of SBSs [32].

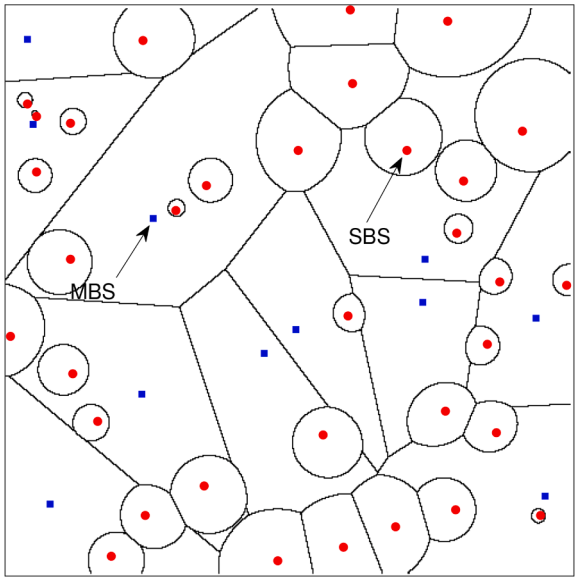

Fig. 1. A two-tier uniform HCN depicting the coverage regions of BSs from both BS tiers.

Nonetheless, another approach that has recently been adopted in numerous research works is focused on adding BSs mounted on unmanned air vehicles (UAVs) in the already deployed terrestrial cellular networks. The deployment of UAV-BSs helps not only in the enhancement of network coverage, but also in accounting for the increased traffic demands especially during the occasional events [33,34]. Owing to their mobility, rapid and low-cost deployments, and reliability, UAV-BSs are expected to be an integral part of the emerging cellular networks. However, the UAV based cellular networks are vastly different from the terrestrial cellular networks as the higher elevation of UAV-BSs mostly results in LoS communication links with the users. Similarly, the characteristics of the UAV-to-ground channel are more complex and different from the typical ground-to-ground (G2G) channel as well. Hence, prior to the successful roll-out of UAV based cellular networks, there is an urgent need to design dedicated and efficient resource management and security mechanisms for UAV communications. Moreover, owing to the flexible mobility of UAVs, effective coordination mechanisms are to be designed that ensure reliable connectivity in multi-UAVs deployment scenarios [35–37]. However, the prime focus of this paper is on the non-uniform densification of static SBSs and relevant state-of-art work is presented in the following passages.

In order to ensure an improved capacity and coverage of the deployed HCN, a simplified non-uniform deployment of SBSs was considered by muting the SBSs within a specific distance away from the MBSs. The prime advantage associated with this spatial separation (achieved through muting of SBSs) between MBSs and SBSs is that it protects the UEs within the exclusion zones (i.e., the MBS cell-center region) from excessive interference caused by the nearby SBSs. A noteworthy improvement in the network coverage and throughput was observed from the uniform SBS deployment scenario and that too at a lower SBS densification i.e., lesser expense [38]. Fazal et al. extended the non-uniform model proposed in [38] by inculcating the load balancing perspective based on SBS biasing [39]. The authors observed considerable improvement in the offloading of UEs at macro cell-edge region using SBS biasing which further improved the utilization of network resources and resulted in capacity enhancement of the non-uniform HCNs (NuHCNs). The selective SBS muting model ensuring load balancing presented in [39] was extended in [40,41] when the load balancing mechanism was studied in conjunction with an interference

management strategy based on reverse frequency allocation (RFA) and soft frequency reuse (SFR) respectively. The joint incorporation of load balancing and interference avoiding strategies further improved the performance of NuHCNs as compared to Wang et al. [38] and Muhammad et al. [39].

Similarly, Deng et al. proposed adding dependencies between locations of MBSs and SBSs, i.e., deploying SBSs only in those regions which are either not completely covered by MBSs or in regions that are relatively far away from MBSs [42]. Another approach available in literature for the non-uniform or selective SBS deployments is based on Stienen's model. The coverage area of an MBS in Stienen's model is divided into two disjoint regions, i.e. MBS cell-center and outside/boundary region. In this model, the MBSs and UEs are distributed using independent PPPs while the SBSs are deployed only in outer region of macro coverage area using poisson hole process (PHP). This selective deployment of SBSs assists in ensuring reduced interference within the MBS cell-center region, and thus helps in achieving improved performance of the deployed network [43]. Sajid et al. have also studied the impact of non-uniform SBS deployments using Stienen's model integrated with SBS biasing and interference abating schemes including RFA and SFA respectively in [44,45].

It is important to mention here that the emerging networks are bound to be dense, especially given their astounding success in meeting the high capacity demands over the past few years. Therefore, to accurately estimate the path losses in such disparent link distance based scenarios, it is important to employ more accurate and realistic path loss models (PLMs) that can efficiently estimate the propagation environment. For instance, by using the standard single-slope (SS) based PLM, the authors reported independence of signal to interference plus noise ratio (SINR) distribution from the network density in fully-loaded HCNs [8,25]. Contrarily, by employing more accurate PLMs, numerous research works have shown that the network coverage is not only sensitive to the SBS densification but the ultra densification of SBSs significantly degrades the network performance as well [46–48]. This contrasting behavior of HCNs is largely because of the SS-PLM, which fails to precisely capture the path loss in dense network deployment scenarios. The SS-PLM works on a '*one-size-fits-all approach*', and its usage may lead to severe differences in estimating the strength of the desired and interfering signals.

2.1. Gap analysis

The available literature on performance analysis of dense NuHCNs is strictly limited to the usage of SS-PLM only [38–45]. While the estimation of path loss using SS-PLM is based on a simplified approach, i.e., the decay rate of a signal is assumed to be uniform over all ranges of the link distance. Due to this assumption, SS-PLM fails to precisely capture the dependence of the value of PLE on the range of link distance in dense cellular networks. Nevertheless, the signal attenuation generally increases with the distance in practical networks due to the presence of numerous obstacles in the path between UEs and BSs [48,49]. Contrarily, the multi-slope PLMs are well-known to be more accurate owing to their innate ability to account for the extensive variations in desired and interfering links [50,51]. Therefore, a more precise PLM based on dual slope (DS) has been employed in this paper to analyze the downlink performance of a two-tier NuHCN. The adopted PLM differentiates between the shorter and larger links by a critical distance, as different values of PLE are considered for each of them.

Moreover, to account for the disparity in transmit powers of both BS tiers, a commonly adopted load balancing strategy based on SBS biasing is also considered. While on the other hand, to ensure that the offloaded UEs from macro tier do not receive intense interference from nearby MBSs and SBSs, a simple interference abating scheme based on traditional frequency reuse is also incorporated. Thus, to the best of our knowledge, this is the first study that analyzes the downlink performance of a multi-tier NuHCN using multi-slope PLM which jointly incorporates the load balancing and interference management perspectives.

By using DS-PLM, the coverage area of a BS is divided into two non-overlapping regions separated by a critical distance and this special distance is well-known to be dependent upon the antenna heights of the communicating stations [52]. For a two-tier HCN in which BSs of both tiers are randomly deployed using two independent PPPs, the SBSs that exist at distances smaller than the critical distance of each MBS are deactivated to form an NuHCN. This selective SBS deactivation ensures that most of the SBSs are deployed at locations where MBSs have weaker coverage. Moreover, the UEs that are located within the critical distance of any MBS are bound to associate with that MBS, as the UEs mostly receive a stronger signal from MBS as compared to the nearest SBS within that distance range [53].

2.2. Major contributions

The primary contributions of this paper are summarized as under:

1. Using DS-PLM, novel expression for the macro association of a random UE is determined for the two-tier NuHCNs. The derived expression clearly highlights the important parameters of UE association with macro tier BSs. Furthermore, it also sheds light on the improved efficiency of SBS biasing in MBS cell-edge/boundary region (post critical distance), as the UEs are proactively offloaded to SBSs in that region which reduces the load from macro tier.
2. New expression for the network coverage probability is derived for the two-tier NuHCNs using DS-PLM, which highlights the dependency of network coverage on BS densities and critical distances of both tiers. Contrary to uniform HCNs, NuHCNs can ensure the same coverage performance with far lesser SBS deployments, owing to the reduction in interference due to selective SBS deployments. Moreover, the coverage performance of NuHCNs also highlights the perks of utilizing load balancing mechanism in conjunction with simple frequency reuse, as the network coverage provided by NuHCNs is significantly greater than the uniform HCNs.

2.3. Paper organization

The remaining sections of the paper are organized in the following manner: In Section 3, the system model adopted in this work along with the details of all assumptions are described. Section 4 presents the analysis for macro tier association probability and statistical distance distributions for communicating distances greater and smaller than macro tier critical distance. The derivation of network coverage probability expression is presented for the two tier NuHCNs in Section 5. The numerical results are presented in Section 6, while the conclusions are drawn in Section 7. The notations used in the paper are enlisted in Table 1.

3. Problem formulation and system model

This paper considers a two-tier BS system comprising of macro and small BSs which are distributed in a service area using distinct PPPs, represented as ϕ_M and ϕ_S respectively. The deployed BSs have distinct spatial densities (λ_M and λ_S) and transmit powers (P_M and P_S) as well, while it is further assumed that $\lambda_S \geq \lambda_M$ and $P_S < P_M$. Besides this, the UEs are also assumed to be distributed through an independent PPP represented as ϕ_{UE} having density λ_U. The analysis is carried out for a T-UE which is assumed to be located at the origin and Silvnyak's Theorem justifies this assumption owing to a special property of PPPs [54].

Using DS-PLM, the power received (S_{DL_i}) by the T-UE at a distance X_i from an ith tier BS is given as,

Table 1
Notations summary .

Notation	Description
ϕ_M, ϕ_S, ϕ_{UE}	PPPs of MBSs, SBSs and UEs, respectively
λ_M, λ_S, λ_U	Spatial densities of MBSs, SBSs and UEs, respectively
P_M, P_S	Transmit powers of MBSs and SBSs, respectively
S_{DL_i}	Power received by the T-UE from ith tier BS
X_i	Distance of T-UE from ith tier BS
R_{C_i}	ith tier critical distance
x_{0_i}	Close-in reference distance for ith tier BS
L_0	Path loss at close-in reference distance
h_{X_i}	Rayleigh fading gain
α_{0i}, α_{1i}	Distance dependent PLEs, $\alpha_{1i} > \alpha_{0i} > 2$
Γ	Instantaneous received SINR
τ	SINR threshold
σ^2	Noise power
B_S	SBS biasing factor
N	Frequency reuse factor
$\mathcal{A}_{\mathcal{M}}$	Macro association probability of T-UE
C_{P_i}	Coverage probability of ith tier

$$S_{DL_i}(x_i) = \begin{cases} P_i h_{X_i} L_0 \left(\frac{x_{0_i}}{x_i}\right)^{\alpha_{0i}} & x_i \leq R_{Ci} \\ P_i h_{X_i} L_0 \left(\frac{x_{0_i}}{R_{Ci}}\right)^{\alpha_{0i}} \left(\frac{R_{Ci}}{x_i}\right)^{\alpha_{1i}} & x_i > R_{Ci}, \end{cases} \tag{1}$$

where the fading coefficient denoted as h_{X_i} is considered to be Rayleigh distributed and its power is exponentially distributed with unity mean, i.e., $h_{X_i} \sim \exp(1)$. Besides this, the close-in reference distance for both BS tiers is represented by $x_{0_i} = 1$m, while the path loss observed at x_{0_i} is denoted by L_0. Moreover, as can be seen from (1), the received power expression ignores shadowing effect and this assumption is considered to improve the tractability of our analysis [7,55]. In contrast to the SS-PLM where signals decay with increasing distance but at a single rate, employing DS-PLM ensures the desired and interfering signals both experience a more realistic distance dependent path loss using dual decay rates. This effectively means that there is a disparity in signal decay rate beyond the BS critical distance R_{Ci}. The far field signal decay rate or the path loss exponent (PLE) for distances smaller than R_{Ci} is represented by α_{0i}, while α_{1i} denotes the PLE for distances farther than R_{Ci}. Typically, the values of these PLEs are greater than 2, i.e.,$\alpha_{1i} > \alpha_{0i} > 2$. While the value of α_{1i} lies in the range [2, 6].

Given dense deployment of SBSs, multiple SBSs can appear in the coverage area of any MBS and thus can badly effect the services offered by MBS to its UEs depending upon their location w.r.t the serving MBS. Therefore, to safeguard the services' quality offered by MBSs to their respective UEs specially in their near-vicinity, an NuHCN is considered in which the SBSs located within the R_{CM} of any MBS are assumed to be muted (as shown in Fig. 2). The UE association policy adopted in this paper is based on maximum average biased received power. Moreover, to account for the disparity in transmit powers of both tiers in NuHCNs, static SBS biasing is also employed to offload UEs from macro to small tier.

It is further assumed that none of the deployed BSs in the NuHCN are unloaded i.e., every BS has some data for its associated UEs. It is important to note that by removing the SBSs from near-vicinity of MBSs, the SBSs are mostly located outside of macro cell-center region. Hence, it is a valid assumption that none of the deployed BSs in the NuHCN are unloaded. Moreover, to ensure that the aggregate interference received by the UEs is reduced substantially, a simple frequency reuse mechanism is incorporated which helps in countering the decrease in received SINRs at UEs due to their offloading from macro tier and excessive SBS densification. The adopted frequency reuse mechanism divides the available bandwidth resource into N equal channels i.e., $F_1, F_2, \ldots, F_N$ while each BS randomly chooses 1 out of N channels. Since, independently thinning out a PPP results into another PPP, thus, the tractability associated with PPP is retained.

The instantaneous received SINR (Γ) at T-UE which is associated with ith tier BS is given as

$$\Gamma_i = \frac{S_{DL_i}}{\sum\limits_{j \,\epsilon\, \{\phi_{M,N} \cup \phi_{S,N}\} \setminus i} S_{DL_j} + \sigma^2}, \tag{2}$$

where σ^2 refers to a constant thermal noise power which is assumed to have an additive nature. Furthermore, $\phi_{M,N} \cup \phi_{S,N}$ represents a collection of all MBSs and SBSs which are operating at the same frequency channel (i.e., N) over which the serving BS of T-UE is operating. Moreover, it is important to note the impact of fading is considered in determining the complementary cumulative distribution function (CCDF) of SINR, though it was ignored in determining of T-AP to avoid ping-pong handoffs.

4. Tier association probability (T-AP) and probability density function (PDF) of distance to the serving BS

In this section, the derivations of macro T-AP expression and distance distributions for each of the association regions i.e., ($X_M > R_{CM}$ and $X_M < R_{CM}$) to the serving MBS are presented. The critical distance based T-UE association regions are given in Table 2.

In a two-dimensional homogeneous PPP, the probability of having no

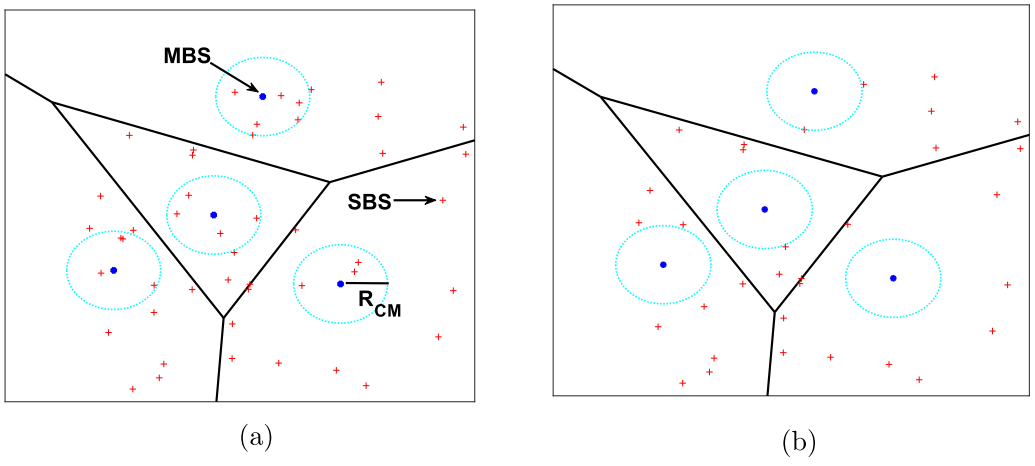

Fig. 2. Conversion of a two-tier uniformly distributed HCN to NuHCN by muting SBSs lying within the critical region of MBSs.

Table 2
Association Regions for T-UE in a two-tier NuHCN .

Regions	Communicating Distance Ranges
R-I	$[X_M < R_{CM}]$
R-II	$[X_M > R_{CM} \cap X_S > R_{CS}]$
R-III	$[X_M > R_{CM} \cap X_S < R_{CS}]$

BS in a circle of radius x_i which is also the distance to the nearest i-th tier BS is given using [56] as,

$$\mathbb{P}[X_i > x_i] = \exp\big(-\pi\lambda_i x_i^2\big). \tag{3}$$

Using (3), the likelihood that the T-UE can be located in any of the association regions (see Table I for region details) of a two-tier NuHCN can be expressed as,

$$\begin{aligned}\mathbb{P}[\text{R-I}] = \varsigma &= 1-\exp\big(-\pi\lambda_M R_{CM}^2\big).\\ \mathbb{P}[\text{R-II}] = \varpi &= \exp\big(-\pi\big(\lambda_M R_{CM}^2+\lambda_S R_{CS}^2\big)\big).\\ \mathbb{P}[\text{R-III}] = \varrho &= \exp\big(-\pi\lambda_M R_{CM}^2\big)-\exp\big(-\pi\big(\lambda_M R_{CM}^2+\lambda_S R_{CS}^2\big)\big).\end{aligned}$$

It is clear from these expressions that the location of T-UE in any of the association regions is dependent on both the tier densities and critical distances. The PDF of X_i where $x_i \geq 0$ can also be expressed using (3) as,

$$f_{X_i}(x_i) = 2\pi\lambda_i x_i \exp\big(-\pi\lambda_i x_i^2\big). \tag{4}$$

4.1. Tier association probability

The association of T-UE with any BS tier is chiefly dependent on BS density, transmit power and distance from the nearest BS of that tier. Using DS-PLM, the importance of distance between the deployed BSs and UEs considerably increases owing to the disparity in estimated path loss (due to different power decay rates) for smaller and larger communicating distances. In accordance with the system model, if the T-UE lies within the R_{CM} of its nearest MBS, then it is forced to associate with it (i.e., the nearest MBS) as all SBSs within the R_{CM} of each MBS are muted. While for the remaining coverage area of the NuHCN, the T-UE association with any BS is solely based on the highest averaged biased received power.

The likelihood that T-UE associates with macro tier in a two-tier NuHCN, when path loss is estimated using DS-PLM is given as,

$$\mathcal{A}_{\mathcal{M}} = \mathcal{A}_{\mathcal{M},R_{\text{OUT}}} + \mathcal{A}_{\mathcal{M},R_{\text{IN}}}, \tag{5}$$

where $\mathcal{A}_{\mathcal{M},R_{\text{OUT}}}$ refers to the T-UE association with macro tier when the nearest MBS is at least apart by R_{CM}, while $\mathcal{A}_{\mathcal{M},R_{\text{IN}}}$ denotes the T-UE association with macro tier when the distance between T-UE and its closest MBS is less than R_{CM}.

4.1.1. Macro association of T-UE inside R_{CM}

When the T-UE is located within the R_{CM} of its nearest neighbor, it is only permitted to associate with it and its likelihood is given using the 2D null probability as:

$$\mathcal{A}_{\mathcal{M},X_M<R_{CM}} = 1-\exp\big(-\pi\,\big(\lambda_M R_{CM}^2\big)\big). \tag{6}$$

It is clear from (6) that the T-UE association probability in R-I is independent of λ_S and R_{CS} as the SBSs within R_{CM} are muted. Moreover, it is interesting to note here that the T-UE association within R_{CM} is not affected by the BS transmit powers and PLEs (pre-critical and post-critical) of both tiers either, as the only dominant factor dictating this likelihood is the R_{CM} which is also the size of exclusion region. As described earlier, when the T-UE is located within the R_{CM} of its nearest MBS, it receives network services from macro tier only. Therefore, the T-UE association with small tier within R-I, i.e., $\mathcal{A}_{\mathcal{S},X_S<R_{CS}} = 0$.

4.1.2. Macro association of T-UE outside R_{CM}

It is the association when the distance between T-UE and its nearest MBS is greater than R_{CM}, and the T-UE still receives higher power from it as compared to the closest SBS even after considering extended cell range of small BS tier. In accordance with the system model, the association probability of T-UE with macro tier falls in two regions i.e., R-II and R-III as given in Table 2.

Propostion 1. The association probability of T-UE with macro tier in R-II is given as,

$$\mathcal{A}_{\mathcal{M},\text{R-II}} = 2\pi\lambda_M \int_{R_{CM}}^{\infty} x_M \begin{cases} e^{\left(-\pi\,\left(\lambda_M x_M^2+\lambda_S(g_1(x_M))^2\right)\right)}\,\mathrm{d}x_M & g_1(x_M)\geq R_{CS}\\ e^{\left(-\pi\,\left(\lambda_M x_M^2+\lambda_S R_{CS}^2\right)\right)}\,\mathrm{d}x_M & g_1(x_M)< R_{CS}\end{cases}, \tag{7}$$

where $g_1(x_M) = (P_S B_S \eta_S / P_M \eta_M)^{1/\alpha_{1S}} x_M^{\alpha_{1M}/\alpha_{1S}}$ and $\eta_i = R_{Ci}^{\alpha_{1i}-\alpha_{0i}}$. It is obvious from (7) that besides λ_i and P_i, the T-UE association probability in R-II is dependent upon α_{1i}, B_S and R_{Ci} as well.

Proof. The joint association probability of T-UE with macro tier in R-II is given by the following probabilistic event

$$\mathcal{A}_{\mathcal{M},\text{R-II}} = \mathbb{P}\big[P_r^{\,M} > P_r^{\,S}, \text{R-II}\big], \tag{8}$$

where $P_r^{\,M}$ and $P_r^{\,S}$ are received powers from the nearest macro and small tier BSs respectively. By using DS-PLM, the averaged received powers from the respective nearest BSs of both tiers in R-II are $P_r^{\,M} = P_M \eta_M L_0 x_M^{-\alpha_{1M}}$ and $P_r^{\,S} = P_S B_S \eta_S L_0 x_S^{-\alpha_{1S}}$ respectively. Inserting them in (8) to get

$$\mathcal{A}_{\mathcal{M},\text{R-II}} = \mathbb{P}[P_M \eta_M L_0 x_M^{-\alpha_{1M}} > P_S B_S \eta_S L_0 x_S^{-\alpha_{1S}},\ \text{R-II}], \tag{9}$$

rearranging the terms in (9) gives

$$\mathcal{A}_{\mathcal{M},\text{R-II}} = \mathbb{P}\left[x_S > \left(\frac{P_S B_S \eta_S}{P_M \eta_M}\right)^{\frac{1}{\alpha_{1S}}} x_M^{\frac{\alpha_{1M}}{\alpha_{1S}}},\ \text{R-II}\right]. \tag{10}$$

From Table 2, we already know the constraints on X_M and X_S in R-II, and based on those distance ranges (10) takes the integral form as

$$\mathcal{A}_{\mathcal{M},\text{R-II}} = \int_{R_{CM}}^{\infty} \mathbb{P}[(x_S > g_1(x_M)\ \cap\ x_S > R_{CS}), \text{R-II}]\, f_{X_M}(x_M)\,\mathrm{d}x_M, \tag{11}$$

where $f_{X_M}(x_M)$ is already given in (4). The integration limits in (11) are from R_{CM} to ∞, as X_M is constrained over the same range as well. Now, simplifying (11) by using (3) gives the desired expression for association probability of T-UE with macro tier in R-II and completes the proof of (7). □

Propostion 2. The association probability of T-UE with macro tier in R-III using DS-PLM is given as:

$$\mathcal{A}_{\mathcal{M},\text{R-III}} = 2\pi\lambda_M \int_{R_{CM}}^{\infty} x_M\, e^{\left(-\pi\lambda_M x_M^2\right)} \left(e^{\left(-\pi\lambda_S \gamma^2\right)} - e^{\left(-\pi\lambda_S R_{CS}^2\right)}\right) \mathrm{d}x_M. \tag{12}$$

where $\gamma = (P_S B_S / P_M \eta_M)^{1/\alpha_{0S}} x_S^{\alpha_{0S}/\alpha_{1M}}$.

Proof. The expression given in Eq. (12) can be derived using the procedure adopted in the derivation of (7). □

Finally, by plugging (6), (7), (12) in (5) we get the complete expression for T-UE macro association probability when DS-PLM is used to estimate the path loss in NuHCN. Moreover, it is clear from the derived expressions of each region that disparity in transmit power of both tiers is the primary reason which creates load imbalance between the BS tiers, and it could be finely tuned by opting subtle values of B_S and R_{CS} as both parameters can assist in proactive offloading of UEs to small tier.

4.2. Distribution of the statistical distances between T-UE and its serving BS for the 2-tier NuHCN

In this subsection, we present the PDFs for T-UE association distances with macro tier w.r.t R_{CM} i.e., for link distances greater and smaller than R_{CM}.

4.2.1. Statistical distance distribution for link distances greater than R_{CM}

Propostion 3. The PDF given T-UE is macro tier associated and located at distances greater than R_{CM} from its nearest MBS is given as

$$f_{X_M|X_M>R_{CM}}(x_M) = \frac{2\pi\lambda_M x_M}{\mathcal{A}_{\mathcal{M},\text{R-II}} + \mathcal{A}_{\mathcal{M},\text{R-III}}} \times \begin{cases} \exp\left(-\pi\left(\lambda_M x_M^2 + \lambda_S (g_1(x_M))^2\right)\right) & g_1(x_M) \geq R_{CS} \\ \exp\left(-\pi\left(\lambda_M x_M^2 + \lambda_S \gamma^2\right)\right) & g_1(x_M) < R_{CS} \end{cases}. \tag{13}$$

Proof. For a macro tier associated T-UE which is located at a distance greater than R_{CM} from its nearest MBS, the likelihood of event $X_M > x_M$ is given as

$$\mathbb{P}[X_M > x_M] = \mathbb{P}[X_M > x_M | (\mathcal{A}_{\mathcal{M}}, X_M > R_{CM})]. \tag{14}$$

Using conditional probability, the right hand side (R.H.S) of (14) can be expressed in terms of a joint probability event as,

$$\mathbb{P}[X_M > x_M] = \frac{\mathbb{P}\left[X_M > x_M, P_r^{\,M} > P_r^{\,S}, X_M > R_{CM}\right]}{\mathbb{P}\left[P_r^{\,M} > P_r^{\,S}, X_M > R_{CM}\right]}, \tag{15}$$

where the denominator in (15) is given by

$$\left[P_r^{\,M} > P_r^{\,S}, X_M > R_{CM}\right] = \mathcal{A}_{\mathcal{M},\text{R-II}} + \mathcal{A}_{\mathcal{M},\text{R-III}}. \tag{16}$$

The integral form of (15) can be expressed as

$$\mathbb{P}[X_M > x_M] = \frac{\int_{x_M}^{\infty} f_{X_M}(x_M)}{\mathcal{A}_{\mathcal{M},\text{R-II}} + \mathcal{A}_{\mathcal{M},\text{R-III}}} \times \mathbb{P}[(X_S > g_1(x_M)) \cap X_S > R_{CS}) \cup (X_S > \gamma \cap X_S \leq R_{CS})]\, \mathrm{d}x_M. \tag{17}$$

where $\gamma = (P_S B_S / P_M \eta_M)^{1/\alpha_{0S}} x_S^{\alpha_{0S}/\alpha_{1M}}$. The proof of PDF of X_M conditioned on link distance between T-UE and associated MBS greater than R_{CM} completes after taking derivative and taking association probability values from equations 11 and 12. No new assumptions were made for simplification. □

4.2.2. Statistical distance distribution for link distances smaller than R_{CM}

Propostion 4. The PDF given T-UE is macro tier associated and located at distances smaller than R_{CM} from its nearest MBS, is given as

$$f_{X_M|X_M<R_{CM}}(x_M) = \frac{2\pi\lambda_M x_M \exp\left(-\pi\lambda_M x_M^2\right)}{1 - \exp\left(-\pi\lambda_M R_{CM}^2\right)}. \tag{18}$$

Proof. The expression in (18) can be easily derived by using the PDF of nearest neighbor distance. □

5. Coverage probability

The T-UE is said to be in network coverage if the received instantaneous SINR from its associated BS is above a predefined threshold τ. The overall network coverage in a two-tier cellular network is the sum of coverages offered by both BS tiers, i.e., $\mathrm{C}_{\mathrm{P}_i}$ and is expressed as

$$\mathbb{C}_{\mathbb{P}} = \sum_{i=1}^{2} \mathrm{C}_{\mathrm{P}_i}. \tag{19}$$

Therefore, for computing the overall network coverage, individual contributions of both macro and small tiers for both regions i.e., $X_i > R_{Ci}$ and $X_i < R_{Ci}$ are to be determined. The coverage probability of tier i can be expressed as

$$\mathrm{C}_{\mathrm{P}_i} = \mathrm{C}_{\mathrm{P}_i|\mathrm{X}_i>\mathrm{R}_{\mathrm{Ci}}} \mathcal{A}_{i,X_i>R_{Ci}} + \mathrm{C}_{\mathrm{P}_i|\mathrm{X}_i<\mathrm{R}_{\mathrm{Ci}}} \mathcal{A}_{i,X_i<R_{Ci}}, \tag{20}$$

where $\mathrm{C}_{\mathrm{P}_i|\mathrm{X}_i>\mathrm{R}_{\mathrm{Ci}}}$ and $\mathrm{C}_{\mathrm{P}_i|\mathrm{X}_i<\mathrm{R}_{\mathrm{Ci}}}$ denote the conditional coverage offered by tier i in both regions respectively, while $\mathcal{A}_{i,X_i>R_{Ci}}$ and $\mathcal{A}_{i,X_i<R_{Ci}}$ represent the joint association probabilities in both regions respectively.

Now by using [25], the probability that T-UE is in coverage, which is equivalent to the CCDF of SINR ($\Gamma_{X_i}(x_i)$) at a distance x_i from its associated ith tier BS can be expressed as

$$\mathbb{P}[\Gamma_{X_i}(x_i) > \tau] = \exp\left(\frac{-\tau\sigma^2}{P_i l(x_i)}\right) \prod_{i \in \{\phi_{M,N} \cup \phi_{S,N}\}} \mathcal{L}_{\mathcal{I}_i}\left(\frac{\tau}{P_i l(x_i)}\right), \tag{21}$$

where $l(x_i)$ refers to the generic path loss function, while $\mathcal{L}_{\mathcal{I}_i}$ denotes the Laplace transform of cumulative interference received at T-UE due to both the inter-tier and co-tier BSs that are operating at frequency channel N.

5.1. Coverage probability of T-UE associated with macro tier

In a two-tier NuHCN, the T-UE can associate with macro tier when its distance is either greater or smaller than the R_{CM}. Therefore, the conditional macro tier coverage for each of the association regions is to be determined and is presented next.

5.1.1. Macro tier coverage when the distance between T-UE and its associated MBS is smaller than R_{CM}

Propostion 5. The macro tier coverage for link distance smaller than R_{CM} corresponds to the coverage likelihood in R-I, and its expression is given in (22).

$$\mathrm{C}_{P_M|X_M<R_{CM}}(x_M) = \int_0^{R_{CM}} \frac{2\pi\lambda_M x_M \exp\left(-\pi\lambda_M x_M^2\right)}{1 - \exp\left(-\pi\lambda_M R_{CM}^2\right)} \times \exp\left(\frac{-\tau\sigma^2}{P_M L_0 x_M^{-\alpha_{0M}}}\right) \exp\left(\frac{-2\pi\lambda_S}{N(-2+\alpha_{1S})}\right) \times \begin{cases} \left(-\frac{P_S \tau \eta_S x_M^{\alpha_{0M}} (R_{CM} - x_M)^{-2+\alpha_{1S}}}{P_M} \times {}_2F_1\left[1, 1-\frac{2}{\alpha_{1S}}; 2-\frac{2}{\alpha_{1S}}; -\frac{P_S \eta_S x_M^{\alpha_{0M}} \tau}{P_M (R_{CM} - x_M)^{\alpha_{1S}}}\right]\right) & x_M \leq R_{CM} - R_{CS} \\ \left(-\frac{P_S \tau \eta_S x_M^{\alpha_{0M}} (R_{CM} + R_{CS} - x_M)^{-2+\alpha_{1S}}}{P_M} \times {}_2F_1\left[1, 1-\frac{2}{\alpha_{1S}}; 2-\frac{2}{\alpha_{1S}}; -\frac{P_S \eta_S x_M^{\alpha_{0M}} \tau}{P_M (R_{CM} + R_{CS} - x_M)^{\alpha_{1S}}}\right]\right) & x_M > R_{CM} - R_{CS} \end{cases} \times \exp\left[\frac{-2\pi\lambda_M}{N}\left(\left(-\frac{x_M^2}{2} {}_2F_1\left[1, \frac{2}{\alpha_{0M}}; 1+\frac{2}{\alpha_{0M}}; -\frac{1}{\tau}\right]\right) + \frac{R_{CM}^2}{2} \times {}_2F_1\left[1, \frac{2}{\alpha_{0M}}; 1+\frac{2}{\alpha_{0M}}; -\left(\frac{R_{CM}}{x_M}\right)^{\alpha_{0M}} \frac{1}{\tau}\right] + \frac{\eta_M \tau x_M^{\alpha_{0M}} (R_{CM})^{2-\alpha_{1M}}}{-2+\alpha_{1M}} \times {}_2F_1\left[1, 1-\frac{2}{\alpha_{1M}}; 2-\frac{2}{\alpha_{1M}}; -\frac{\eta_M \tau (x_M)^{\alpha_{0M}}}{(R_{CM})^{\alpha_{1M}}}\right]\right)\right] \mathrm{d}x_M. \tag{22}$$

Proof. The integral form of macro tier coverage in R-I is given as

$$\mathrm{C}_{P_M|X_M<R_{CM}}(x_M) = \int_0^{R_{CM}} \mathbb{P}\left[\Gamma_{X_{M|X_M<R_{CM}}}(x_M) > \tau\right] f_{X_M|X_M<R_{CM}}(x_M)\, \mathrm{d}x_M, \tag{23}$$

where $f_{X_M|X_M<R_{CM}}(x_M)$ is already determined in Section 4.2 and is given in (18), while $\mathbb{P}[\Gamma_{X_{M|X_M<R_{CM}}}(x_M) > \tau]$ is yet to be derived. The limits of integration in (23) are from 0 to R_{CM} as the T-UE lies at distances smaller than R_{CM} of its closest MBS.

The conditioned macro tier CCDF given x_M smaller than R_{CM} can be expressed with the help of (21) as

$$\mathbb{P}\left[\Gamma_{X_{M|X_M<R_{CM}}}(x_M) > \tau\right] = \exp\left(\frac{-\tau\sigma^2 x_M^{-\alpha_{0M}}}{P_M L_0}\right)\mathcal{L}_{\mathcal{I}_{\mathcal{M}}}\left(\frac{-\tau\, x_M^{\alpha_{0M}}}{P_M}\right)\mathcal{L}_{\mathcal{I}_S}\left(\frac{-\tau\, x_M^{\alpha_{0M}}}{P_M}\right). \tag{24}$$

In region x_M smaller than R_{CM}, the T-UE can possibly receive co-tier interference from MBSs operating at frequency channel N and located at distances both greater and smaller than R_{CM}. Therefore, $\mathcal{L}_{\mathcal{I}_{\mathcal{M}}}$ for x_M smaller than R_{CM} contains two integrals in its expression

$$\mathcal{L}_{\mathcal{I}_{\mathcal{M}}}\left(\frac{-\tau\, x_M^{\alpha_{0M}}}{P_M}\right) = \exp\left(\frac{-2\pi\lambda_M}{N}\left(\int_{x_M}^{R_{CM}} \frac{y}{1+(x_M^{\alpha_{0M}}\tau)^{-1}y^{\alpha_{0M}}}\mathrm{d}y + \int_{R_{CM}}^{\infty} \frac{y}{1+(x_M^{\alpha_{0M}}\eta_M\tau)^{-1}y^{\alpha_{1M}}}\mathrm{d}y\right)\right) \tag{25}$$

Solving the integration in (25), we get

$$\mathcal{L}_{\mathcal{I}_{\mathcal{M}}}\left(\frac{-\tau\, x_M^{\alpha_{0M}}}{P_M}\right) = \exp\left[\frac{-2\pi\lambda_M}{N}\left(\left(-\frac{x_M^2}{2}\,{}_2F_1\left[1,\frac{2}{\alpha_{0M}};1+\frac{2}{\alpha_{0M}};-\frac{1}{\tau}\right]\right)\right.\right.$$
$$\left.+\frac{R_{CM}^2}{2}\,{}_2F_1\left[1,\frac{2}{\alpha_{0M}};1+\frac{2}{\alpha_{0M}};-\left(\frac{R_{CM}}{x_M}\right)^{\alpha_{0M}}\frac{1}{\tau}\right]\right)$$
$$\left.+\frac{\eta_M\tau x_M^{\alpha_{0M}}{}^{!}\text{"substring}-after(preceding-sibling::comment()[starts-with(.,'hskip')][1],'hskip')\text{"}pt>(R_{CM})^{2-\alpha_{1M}}}{-2+\alpha_{1M}}\,{}_2F_1\left[1,1-\frac{2}{\alpha_{1M}};2-\frac{2}{\alpha_{1M}};-\frac{\eta_M\tau(x_M)^{\alpha_{0M}}}{(R_{CM})^{\alpha_{1M}}}\right]\right)\right] \tag{26}$$

The integration limits for determining the inter-tier interference in region x_M smaller than R_{CM} is a little tricky. This is because, we need to ensure that the T-UE associates with MBS when it lies inside the R_{CM} of its closest MBS. Moreover, given $x_M < R_{CM}$, there is a very little likelihood that the T-UE may still receive better signal strength from SBSs residing near the R_{CM} boundary of MBS. Therefore, to avoid such a scenario, we take small tier interference with reference to x_M, i.e., $x_M \le (R_{CM}-R_{CS})$ or $x_M > (R_{CM}-R_{CS})$. The integral form of inter-tier interference is given as

$$\mathcal{L}_{\mathcal{I}_S}\left(\frac{-\tau\, x_M^{\alpha_{0M}}}{P_M}\right) = \exp\left(\frac{-2\pi\lambda_S}{N}\right.$$
$$\left.\times\begin{cases}\left(\int_{(R_{CM}-x_M)}^{\infty}\frac{y}{1+\left(x_M^{\alpha_{0M}}\frac{P_S\eta_S}{P_M}\tau\right)^{-1}y^{\alpha_{1S}}}\mathrm{d}y\right) & x_M \le R_{CM}-R_{CS}\\ \left(\int_{(R_{CM}+R_{CS}-x_M)}^{\infty}\frac{y}{1+\left(x_M^{\alpha_{0M}}\frac{P_S\eta_S}{P_M}\tau\right)^{-1}y^{\alpha_{1S}}}\mathrm{d}y\right) & x_M > R_{CM}-R_{CS}\end{cases}\right) \tag{27}$$

Simplifying (27) by using appropriate substitution to get

$$\mathcal{L}_{\mathcal{I}_S}\left(\frac{-x_M^{\alpha_{0M}}\tau}{P_M}\right) = \exp\left(\frac{-2\pi\lambda_S}{N(-2+\alpha_{1S})}\right.$$
$$\left.\times\begin{cases}\left(-\frac{P_S\tau\eta_S x_M^{\alpha_{0M}}(R_{CM}-x_M)^{-2+\alpha_{1S}}}{P_M} \times {}_2F_1\left[1,1-\frac{2}{\alpha_{1S}};2-\frac{2}{\alpha_{1S}};-\frac{P_S\eta_S x_M^{\alpha_{0M}}\tau}{P_M(R_{CM}-x_M)^{\alpha_{1S}}}\right]\right) & x_M \le R_{CM}-R_{CS}\\ \left(-\frac{P_S\tau\eta_S x_M^{\alpha_{0M}}(R_{CM}+R_{CS}-x_M)^{-2+\alpha_{1S}}}{P_M} \times {}_2F_1\left[1,1-\frac{2}{\alpha_{1S}};2-\frac{2}{\alpha_{1S}};-\frac{P_S\eta_S x_M^{\alpha_{0M}}\tau}{P_M(R_{CM}+R_{CS}-x_M)^{\alpha_{1S}}}\right]\right) & x_M > R_{CM}-R_{CS}\end{cases}\right) \tag{28}$$

The resultant expression for macro tier contribution in CCDF of the received SINR for x_M smaller than R_{CM} is obtained by inserting (26) and (28) in (24) to get

$$\mathbb{P}\left[\Gamma_{X_{M|X_M<R_{CM}}}(x_M) > \tau\right] = \exp\left(\frac{-\tau\sigma^2}{P_M L_0 x_M^{-\alpha_{0M}}}\right)\exp\left(\frac{-2\pi\lambda_S}{N(-2+\alpha_{1S})}\right.$$
$$\left.\times\begin{cases}\left(-\frac{P_S\tau\eta_S x_M^{\alpha_{0M}}(R_{CM}-x_M)^{-2+\alpha_{1S}}}{P_M} \times {}_2F_1\left[1,1-\frac{2}{\alpha_{1S}};2-\frac{2}{\alpha_{1S}};-\frac{P_S\eta_S x_M^{\alpha_{0M}}\tau}{P_M(R_{CM}-x_M)^{\alpha_{1S}}}\right]\right) & x_M \le R_{CM}-R_{CS}\\ \left(-\frac{P_S\tau\eta_S x_M^{\alpha_{0M}}(R_{CM}+R_{CS}-x_M)^{-2+\alpha_{1S}}}{P_M} \times {}_2F_1\left[1,1-\frac{2}{\alpha_{1S}};2-\frac{2}{\alpha_{1S}};-\frac{P_S\eta_S x_M^{\alpha_{0M}}\tau}{P_M(R_{CM}+R_{CS}-x_M)^{\alpha_{1S}}}\right]\right) & x_M > R_{CM}-R_{CS}\end{cases}\right)$$
$$\times\exp\left[\frac{-2\pi\lambda_M}{N}\left(\left(-\frac{x_M^2}{2}\,{}_2F_1\left[1,\frac{2}{\alpha_{0M}};1+\frac{2}{\alpha_{0M}};-\frac{1}{\tau}\right]\right)\right.\right.$$
$$\left.+\frac{R_{CM}^2}{2}\,{}_2F_1\left[1,\frac{2}{\alpha_{0M}};1+\frac{2}{\alpha_{0M}};-\left(\frac{R_{CM}}{x_M}\right)^{\alpha_{0M}}\frac{1}{\tau}\right]\right.$$
$$\left.\left.+\frac{\eta_M\tau x_M^{\alpha_{0M}}(R_{CM})^{2-\alpha_{1M}}}{-2+\alpha_{1M}}\,{}_2F_1\left[1,1-\frac{2}{\alpha_{1M}};2-\frac{2}{\alpha_{1M}};-\frac{\eta_M\tau(x_M)^{\alpha_{0M}}}{(R_{CM})^{\alpha_{1M}}}\right]\right)\right] \tag{29}$$

Lastly by inserting (29) into (23), we get the desired expression for macro tier coverage in R-I to complete the proof of (22). □

5.1.2. Macro tier coverage when the distance between T-UE and its associated MBS is greater than R_{CM}

Propostion 6. The macro tier coverage for link distance greater than R_{CM} corresponds to the cumulative likelihood in UE association regions R-II and R-III. The resultant expression for $x_M > R_{CM}$ is given in (30).

$$C_{P_M|X_M>R_{CM}}(x_M)=\int_{R_{CM}}^{\infty}\frac{2\pi\lambda_M x_M}{\mathcal{A}_{\mathcal{M},\text{R-II}}+\mathcal{A}_{\mathcal{M},\text{R-III}}}\left(\exp\left(\frac{-\tau\sigma^2}{P_M\eta_M L_0 x_M^{-\alpha_{1M}}}\right)\times\exp\left(\frac{-2\pi\lambda_M\tau x_M^2}{N(-2+\alpha_{1M})}{}_2F_1\left[1,1-\frac{2}{\alpha_{1M}};2-\frac{2}{\alpha_{1M}};-\tau\right]\right)\right)$$

$$\times\begin{cases}\exp\left(\frac{-2\pi\lambda_S\tau(g_1(x_M))^2}{N(-2+\alpha_{1S})}{}_2F_1\left[1,1-\frac{2}{\alpha_{1S}};2-\frac{2}{\alpha_{1S}};-\frac{\tau}{B_S}\right]\right)\\ \quad\times\exp\left(-\pi\left(\lambda_M x_M^2+\lambda_S g_1(x_M)^2\right)\right)\mathrm{d}x_M & g_1(x_M)\geq R_{CS}\\ \exp\left(\frac{-2\pi\lambda_S}{N}\left(\frac{(g_0(x_M))^2}{2}{}_2F_1\left[1,\frac{2}{\alpha_{0S}};1+\frac{2}{\alpha_{0S}};-\frac{B_S}{\tau}\right]\right.\right.\\ \left.+\frac{R_{CS}^2}{2}{}_2F_1\left[1,\frac{2}{\alpha_{0S}};1+\frac{2}{\alpha_{0S}};-\frac{P_M\eta_M(R_{CS})^{\alpha_{0S}}}{P_S\tau(x_M)^{\alpha_{1M}}}\right]+\frac{P_S B_S\tau x_M^{\alpha_{1M}}}{P_M\eta_M(-2+\alpha_{0S})}\right.\\ \left.\left.\times\left(R_{CS}^{2-\alpha_{0S}}\right){}_2F_1\left[1,1-\frac{2}{\alpha_{0S}};2-\frac{2}{\alpha_{0S}};-\frac{P_S B_S\tau(x_M)^{\alpha_{1M}}}{P_M\eta_M(R_{CS})^{\alpha_{0S}}}\right]\right)\right)\\ \quad\times\exp\left(-\pi\left(\lambda_M x_M^2+\lambda_S R_{CS}^2+\lambda_S\left(\frac{P_S B_S}{P_M\eta_M}\right)^{\frac{2}{\alpha_{0S}}}x_S^{\frac{2\alpha_{0S}}{\alpha_{1M}}}\right)\right)\mathrm{d}x_M & g_1(x_M)<R_{CS}\end{cases}\tag{30}$$

where $g_0(x_M)=(P_S B_S/P_M\eta_M)^{1/\alpha_{0S}}x_M^{\alpha_{1M}/\alpha_{0S}}$ and $g_1(x_M)=(P_S B_S\eta_S/P_M\eta_M)^{1/\alpha_{1S}}x_M^{\alpha_{1M}/\alpha_{1S}}$.

Proof. Please refer to Appendix A. □

Similarly, the expressions for small tier coverage can also be derived using the above procedure. Moreover, for determining the conditional coverage of macro tier, the derived integral-based expressions presented in (22) and (30) for both regions can be numerically evaluated. In addition to this, the complete network coverage expression is determined from (19) when the respective conditional coverage expressions of both tiers are multiplied with their regional association probabilities. Finally, it is important to note that the network coverage analysis using DS-PLM does not introduce any additional complexity in computation, as the number of integrals in SS-PLM and DS-PLM based analysis are the same. Therefore, the DS-PLM based analysis is more useful as compared to the simplistic scenario based on SS-PLM, as it gives valuable design insights without involving additional complexities in computation.

6. Analysis of results

The analytical expressions for the tier association and coverage probabilities have been derived in Sections 4 and 5 respectively. In this section, the accuracy of derived expressions for both performance metrics is validated thorough Monte Carlo simulations. The simulation setup involves placing the T-UE at origin, while the MBS and SBS locations are generated 10^6 times using independent PPPs to ensure all possible BS location possibilities. Furthermore, for ensuring coverage-centric SBS deployments, the SBSs are placed only in those regions where MBSs have either poor or limited coverage. This selective SBS positioning is achieved by assuming that the SBSs lying within the R_{CM} of any MBS are removed or deactivated. Hence, a thinned density of SBSs is considered for the coverage analysis, while original density is assumed for T-AP as all SBSs were available for UEs association. Moreover, for generating the numerical results in this paper, all necessary parametric values considered are as follows: P_M= 53 dBm, P_S= 33 dBm, R_{CM}= 300m,R_{CS}= 55m, B_M= 0 dB, $\alpha_{0M}=\alpha_{0S}$= 2.7, $\alpha_{1M}=\alpha_{1S}$= 3.9, L_0= -32.9 dB and σ^2= -104 dBm.

In order to investigate the performance of DS-PLM based two-tier NuHCN, and for an extensive comparison, we compare the results for both performance metrics with DS-PLM based uniform HCNs and SS-PLM based NuHCNs as well.

6.1. Tier association probability

In this subsection, the validation of macro T-AP analysis for the two-tier NuHCN using DS-PLM is presented initially, while the estimated macro T-AP results are further compared with the SS-PLM based NuHCNs. Moreover, a similar comparison is presented for a CRE-based UE association policy as well.

6.1.1. Validation of macro T-AP analysis and comparison with other system scenarios

For a two-tier NuHCN, a comparison of macro T-AP estimated using SS-PLM and DS-PLM for varying the SBS densification factor (λ_S/λ_M) is depicted in Fig. 3(a). It can be readily observed from the figure that the analytical and simulation results for the DS-PLM are in complete agreement with each other and thus, it validates the correctness of T-AP analysis.

Besides this, it is also evident from the figure that the UEs association with macro tier decreases with the increase in λ_S owing to the decrease in distance between UEs and their nearby SBSs. Though, this decrease in distance certainly ensures improved signal strength from SBSs but the SS-PLM clearly overestimates the UEs association with small tier due to the simplistic approach of assuming a fixed signal degradation rate for all distance ranges. Contrarily, the DS-PLM adopts a relatively more realistic strategy based on disparent path loss, to account for the inhomogeneous signal attenuations over varying communicating distances. Consequently, it estimates the UEs association with any BS tier more precisely when compared with the SS-PLM. For instance, it can be seen from the figure that at $\lambda_S = 50\lambda_M$, around 34% of the UEs associate with macro tier as estimated by SS-PLM while the DS-PLM predicts it to be 45% approximately. Thus, the SS-PLM clearly underestimates the UE access load on macro tier. Moreover, it is also evident from the figure that the UEs association with macro tier is dependent on R_{CS} size as well.

For a detailed insight of UEs association with macro tier using DS-PLM, region-wise UEs association is plotted in Fig. 3(b) against the varying SBS densification factor. It can be seen from the figure that when UEs lie within the R_{CM} of any MBS, they associate with macro tier only without taking into consideration the received power level from their respective nearest SBSs. While it can also be observed from the figure that UEs prefer associating with small tier whenever the distance from the respective nearest SBS is smaller than R_{CS} owing to the higher received power level from them. Moreover, the UEs mostly receive higher signal strength from their proximate MBSs at small λ_S values due to two major reasons i.e., 1) difference in transmit powers of both BS tiers, 2) the distance between UEs and their respective closest SBSs is usually greater than R_{CS}. Consequently, the need for effective UE steering strategies is highlighted to reduce the UE access burden off macro tier.

6.1.2. Impact of SBS biasing on T-AP in NuHCNs

The disparity in transmit power of BS tiers is the principal cause of load imbalance between BS tiers in uniform HCNs, and it is no different in case of NuHCNs as well. Thus, to account for this difference, static SBS biasing is employed to offload UEs to small BS tier. It is clear from Fig. 4 that the SBS biasing helps in offloading UEs to smaller tier which reduces the UE access load on macro tier. It is also evident from the figure that SBS biasing is more effective at relatively lower SBS densification factor. This is because at smaller values of λ_S/λ_M, the UEs mostly lie at distances greater than R_{CS} from their nearest SBSs. Moreover, the transmit power disparity between both BS tiers also paves the way for macro tier

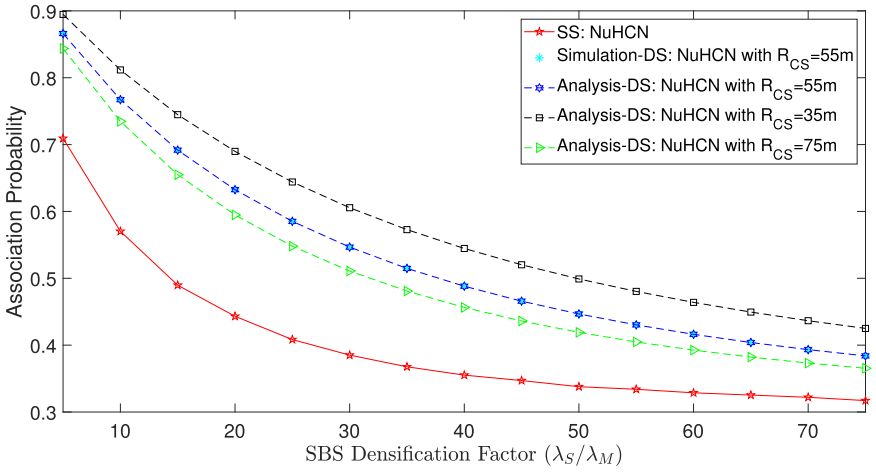

(a)

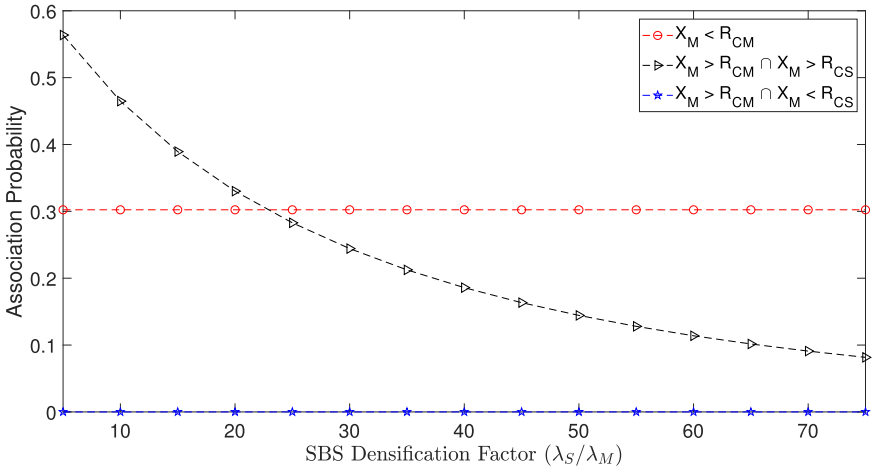

(b)

Fig. 3. Comparison of macro T-AP against varying small tier density.

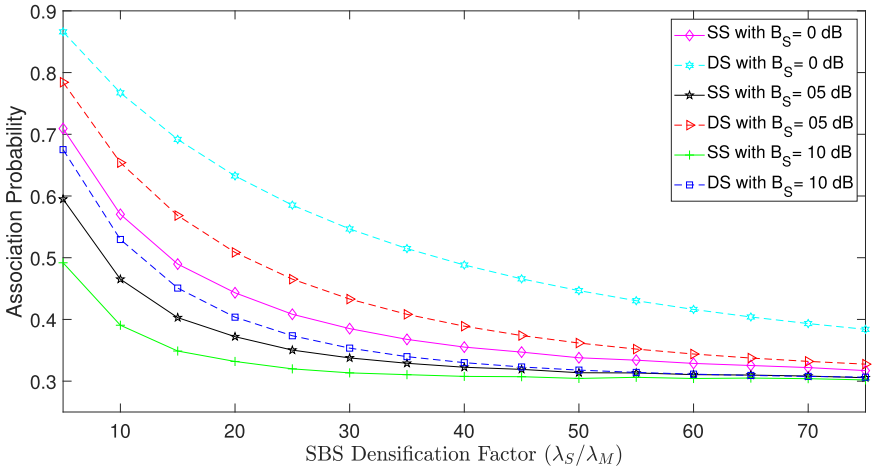

Fig. 4. Comparison of macro T-AP in NuHCNs for both unbiased and biased UE associations.

association of UEs. Contrarily, with the consideration of SBS biasing, the association region of SBSs remarkably enhances (as MBSs are far from SBSs) which helps in steering of UEs towards smaller BS tier.

The SS-PLM usage leads to inaccurate estimation of the load served by any BS tier especially in dense deployment scenarios. Therefore, employing SBS biasing in conjunction with SS-PLM only adds to the error in estimation of the UE access load served by various BS tiers. While DS-PLM is relatively more accurate in estimating the tier load as compared to SS-PLM, hence, it lends same accuracy in the case of biased UE-AS as well. For instance at $\lambda_S = 25\lambda_M$ with B_S=10 dB, the macro T-AP

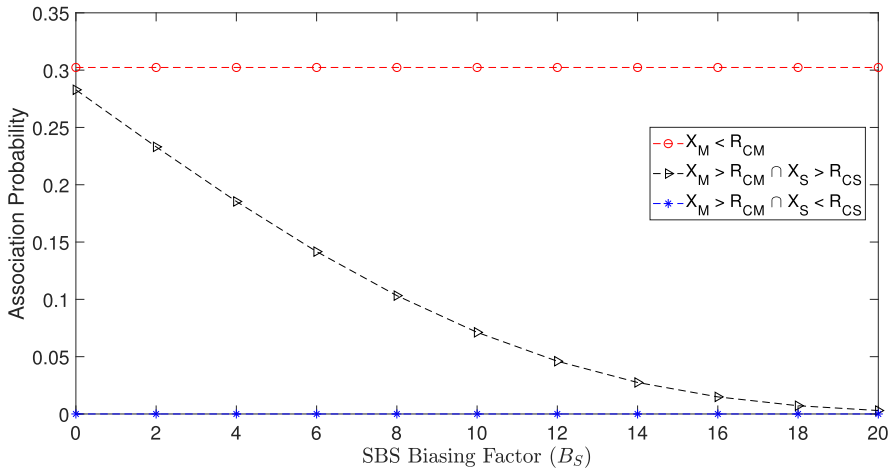

Fig. 5. Impact of SBS biasing on region-based macro T-AP in DS-PLM based NuHCNs.

of UEs estimated by SS-PLM decreases by 33%, while in case of DS-PLM, the macro T-AP decreases by 56%. Moreover, for determining the impact of SBS biasing in all UE association regions of the two-tier NuHCN, Fig. 5 is plotted. It is clear from the figure that whenever T-UE falls within the R_{CM} of its nearest MBS, increasing B_S has no impact on the macro T-AP in that region. This is because, the macro T-AP within the R_{CM} (i.e., the inhibition region for SBSs) is independent of the received power from nearby SBSs. Contrarily, increasing the biasing factor when the distance between T-UE and the nearest MBS is greater than R_{CM}, the macro T-AP swiftly decreases owing to the increase in size of SBS association regions. These observations categorically suggest that the utility of employing biased UE-AS was underestimated by using SS-PLM.

6.2. *Coverage probability*

In this subsection, the validation of network coverage analysis is presented firstly and it is followed by various comparisons of the results

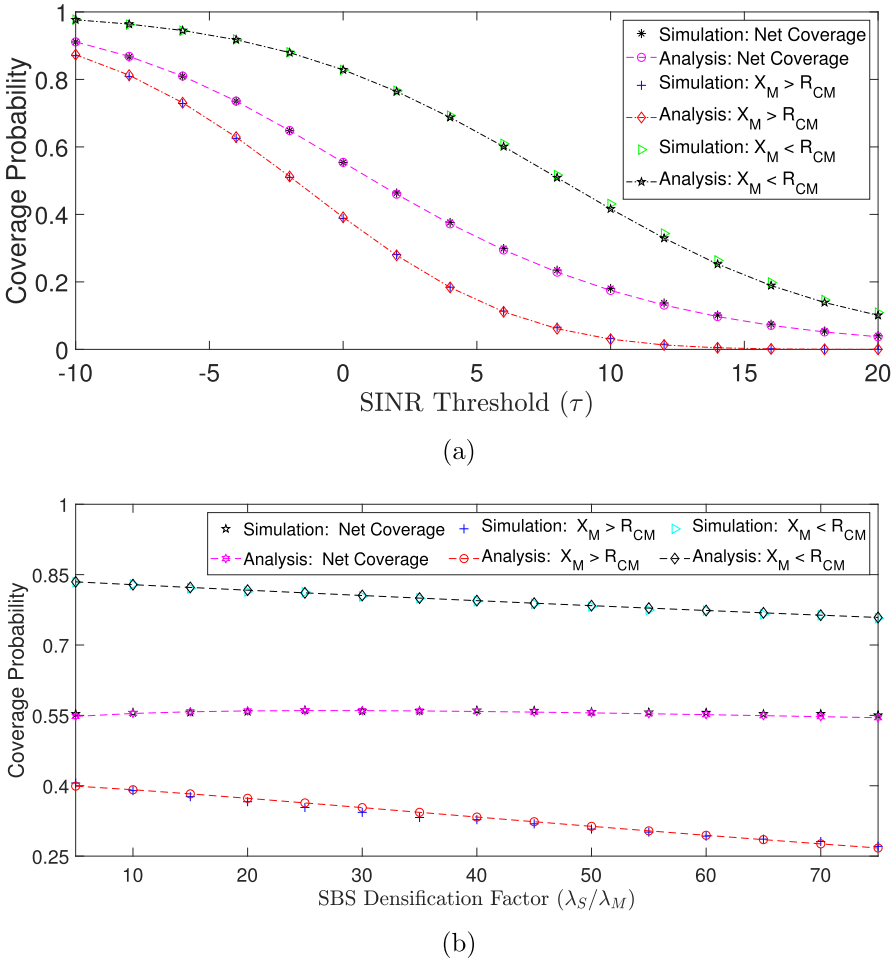

Fig. 6. Validation of network coverage analysis against varying (a) SINR threshold and (b) Small tier density .

achieved for coverage probability through DS-PLM based NuHCNs with multiple system scenarios including SS-PLM based uniform and NuHCNs and DS-PLM based uniform HCNs. Moreover, the individual and joint impact of incorporating SBS biasing and traditional frequency reuse mechanisms in DS-PLM based NuHCNs is also investigated, and it is further compared with other system scenarios as discussed above.

6.2.1. Validation of coverage analysis

In order to validate the coverage analysis, the estimated results are plotted against varying SINR threshold, τ and SBS densification factor, λ_S/λ_M in Fig. 6(a) and (b) respectively. It is evident from both the figures that the analytical results are reasonably consistent with the simulation results. Hence, the derived analytical expression for coverage probability can be used to predict the performance trends and in obtaining critical system design insights as well.

6.2.2. Performance comparison of network coverage with other system scenarios

The impact of varying SBS densification factor (λ_S/λ_M) on the network coverage estimated through different system scenarios based on SS-PLM and DS-PLM is depicted in Fig. 7. It can be observed from the figure that the network coverage in case of SS-PLM based uniform HCNs is independent of variation in λ_S. This is because, the increase in received signal strength due to the increasing SBS density is counter balanced by the rise in interfering signal strength. Contrarily, given better accuracy of DS-PLM in estimating the path loss especially in dense networks, the SINR distribution in DS-PLM based uniform HCNs is found to be a monotonically decreasing function of λ_S. However, with the consideration of SBS thinning (i.e., dependent), the strongest interferers in the vicinity of MBSs are muted and as a result, the overall network coverage improves in both SS-PLM and DS-LM scenarios. For instance at $\lambda_S = 50\lambda_M$ and $\tau = 0$ dB, thinning out the selective SBSs improves the coverage by 6% in SS-PLM scenario while by 9% in DS-PLM. Hence, using SS-PLM underestimates the benefit associated with non-uniform deployment of SBSs in HCNs.

6.2.3. Impact of SBS biasing and frequency reuse on network coverage

Given better accuracy of DS-PLM in estimating the path loss in dense HCNs, and for a fair assessment of determining the impact of utilizing SBS biasing and interference management on network coverage, Figs. 8 and 9 depict a region-wise macro-tier coverage estimated using DS-PLM for both uniform HCNs and NuHCNs.

It can be observed from Fig. 8 that adopting biased UE-AS is advantageous in NuHCNs, as the overall network coverage increases. Contrarily, the coverage reduces with the consideration of biased UE-AS in uniform HCNs as the offloaded UEs receive strong interference from their nearby MBSs. For instance at λ_S=50λ_M, τ = 0 dB, and B_S= 5 dB, the macro-tier cell-edge region coverage increases by around 14% while the overall network coverage in NuHCNs improves by 10%. The non-uniform deployment of SBSs achieved through muting the SBSs within the R_{CM} of each MBS has ensured that only those UEs are offloaded to small-tier BSs which are located far away from their nearest MBS and as a result, receive weak interference from their nearby MBSs.

To account for the excessive interference received at UEs either due to the densification of SBSs or UE offloading, traditional frequency reuse mechanism has been considered. Fig. 9 illustrates that with the usage of frequency reuse mechanism, the number of potential interferers is decreased and as a result, the overall coverage in both uniform HCNs and NuHCNs increases. However, using the frequency reuse mechanism in NuHCNs yields more gain when compared with the uniform HCNs. For instance at λ_S= 50λ_M, τ= 0 dB and N= 3, the network coverage estimated using DS-PLM in NuHCNs is 3% higher than the uniform HCNs. Moreover, it can also be observed that the consideration of frequency reuse has approximately same impact on both the cell-center and cell-edge regions of macro tier.

To highlight the impact of jointly considering the incorporation of both SBS biasing and frequency reuse mechanisms on the region-wise macro-tier coverage estimated using DS-PLM for both uniform HCNs and NuHCNs, Fig. 10 is presented. It can be seen from the figure that the joint incorporation of both mechanisms in conjunction with non-uniform deployment of SBSs results in a 4% increase in the overall network coverage. Moreover, it is also evident from the figure that the joint incorporation of both mechanisms have a little impact on macro-tier coverage for cell-center region, while in case of cell-edge region, the coverage improves by around 5%.

7. Conclusion

In this paper, the downlink performance of a two-tier non-uniform HCN has been analyzed using a more realistic PLM based on dual-slope that effectively accounts for the disparent link distances in dense network scenarios. Due to the transmit power disparity between MBSs and SBSs, the SBSs that fall within the R_{CM} of any MBS have been muted as their likelihood of being active BSs is negligible. By introducing this

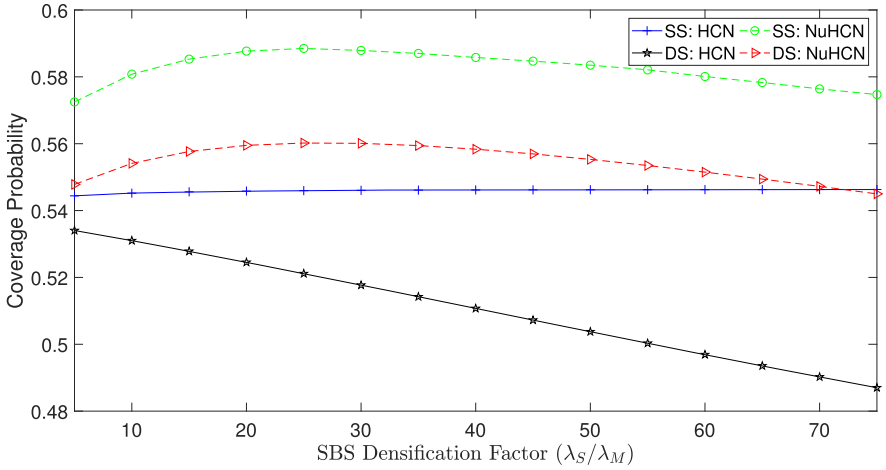

Fig. 7. Network coverage against varying SBS densification factor (λ_S/λ_M).

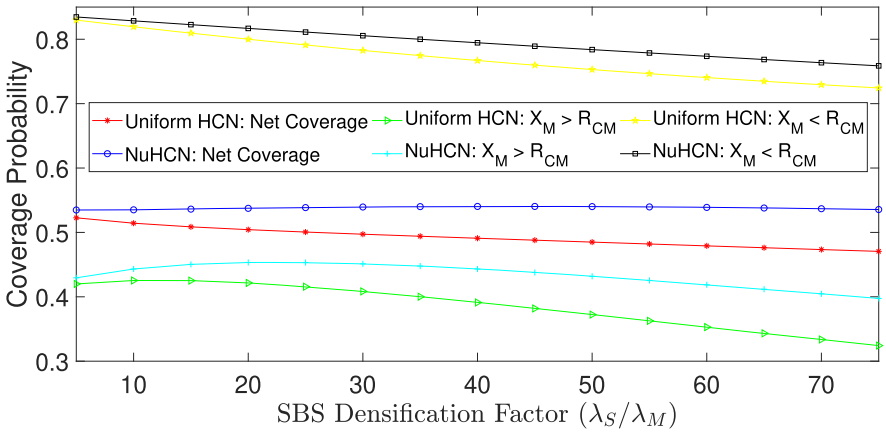

Fig. 8. Coverage comparison for SBS-biasing in uniform HCNs and NuHCNs.

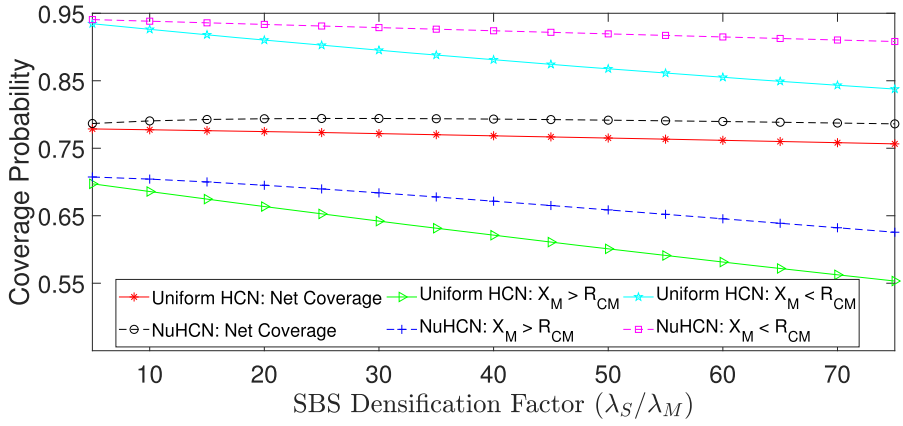

Fig. 9. Coverage comparison with the consideration of frequency reuse mechanism in uniform HCNs and NuHCNs.

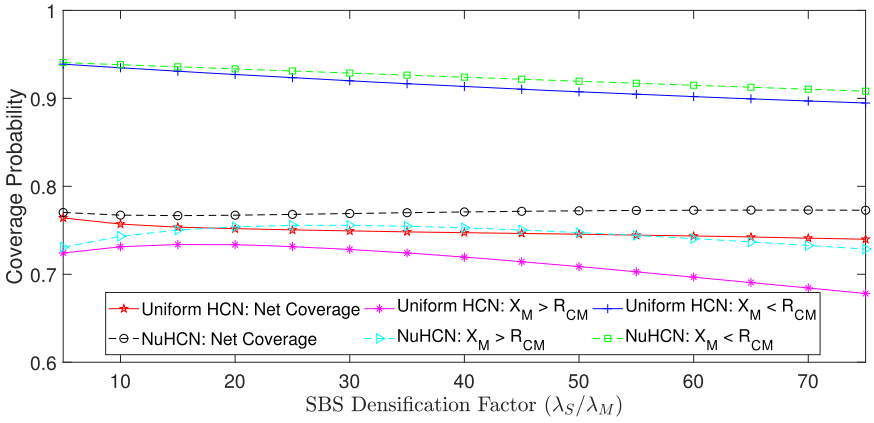

Fig. 10. Coverage comparison with the joint integration of SBS biasing and frequency reuse mechanisms in uniform HCNs and NuHCNs.

correlation between the locations of MBSs and SBSs, the excessive interference received by macro associated users residing in the cell-center region reduces significantly which leads to a substantial improvement in the network coverage. Moreover, the presented model of coverage-centric HCNs has been further studied with the consideration of SBS offloading and interference mitigation mechanisms. The obtained results of the proposed scheme have been compared with other uniform and non-uniform HCNs based on SS-PLM and DS-PLM respectively. It has been observed that the usage of SS-PLM leads to inaccurate estimation of the benefits associated with UE offloading and interference mitigation mechanisms in HCNs. It is pertinent to mention that when the density of SBSs approaches the density of UEs and a fully-loaded system

is considered, then it is necessary to relax the assumption of macro tier association for UE distances less than R_{CM}. This is because, the signal strength received from the nearby SBSs significantly increase in such a scenario, and as a result, the UEs prefer association with the small tier BSs. Nevertheless, the possible extensions of the proposed strategy include a joint consideration of practical load-aware UE association strategies along with spectrally efficient interference management schemes. Similarly, the proposed work can be extended by employing dependent/repulsive point processes to better characterize the locations of BSs in a multi-tier cellular network scenario.

CRediT authorship contribution statement

Khurram Shehzad: Conceptualization, Methodology, Software, Data curation, Investigation, Visualization, Writing - original draft, Formal analysis. **Noor M Khan:** Conceptualization, Methodology, Investigation, Visualization, Supervision, Resources, Validation, Writing - review & editing. **Junaid Ahmed:** Conceptualization, Methodology, Software, Data curation, Supervision, Resources, Validation, Writing - review & editing.

Declaration of Competing Interest

None.

Appendix A. Macro tier coverage when the distance between T-UE and its associated MBS is greater than R_{CM}

The macro tier coverage for link distance X_M greater than R_{CM} is given by the following integral equation as

$$\mathrm{C}_{P_M|X_M>R_{CM}}(x_M) = \int_{R_{CM}}^{\infty} \mathbb{P}\left[\Gamma_{X_{M|X_M>R_{CM}}}(x_M) > \tau\right] f_{X_M|X_M>R_{CM}}(x_M)\, \mathrm{d}x_M, \tag{A.1}$$

where $f_{X_M|X_M>R_{CM}}(x_M)$ is already determined in Section 4.2 and is given in (13), while $\mathbb{P}[\Gamma_{X_{M|X_M>R_{CM}}}(x_M) > \tau]$ is yet to be derived. The limits of integration in (A.1) are from R_{CM} to ∞, as the distance between T-UE and closest MBS (to which the T-UE associates) is greater than R_{CM}.

Using (21) and by substituting the respective parametric values, the CCDF conditioned on X_M greater than R_{CM} can be expressed as

$$\mathbb{P}\left[\Gamma_{X_M|X_M>R_{CM}}(x_M) > \tau\right] = \exp\left(\frac{-\tau\sigma^2 x_M^{\alpha_{1M}}}{P_M\eta_M L_0}\right)\mathcal{L}_{\mathcal{I}_{\mathcal{M}}}\left(\frac{\tau\, x_M^{\alpha_{1M}}}{P_M\eta_M}\right)\mathcal{L}_{\mathcal{I}_{\mathcal{S}}}\left(\frac{\tau\, x_M^{\alpha_{1M}}}{P_M\eta_M}\right). \tag{A.2}$$

In (A.2), the cumulative effect of co-tier and inter-tier interference is to be determined and Laplace Transform is used to determine their contributions. Moreover, it is important to note here that only those BSs from both tiers interfere with the reference link that are operating at frequency channel i.e., N. Using Campbell Mecke theorem and probability generating functional (PGFL) of PPP, the Laplace transform of co-tier interference $\mathcal{L}_{\mathcal{I}_{\mathcal{M}}}$ is given as

$$\mathcal{L}_{\mathcal{I}_{\mathcal{M}}}\left(\frac{\tau\, x_M^{\alpha_{1M}}}{P_M\eta_M}\right) = \exp\left(\frac{-2\pi\lambda_M}{N}\int_{x_M}^{\infty}\frac{y}{1+(x_M^{\alpha_{1M}}\tau)^{-1}y^{\alpha_{1M}}}\mathrm{d}y\right). \tag{A.3}$$

The integration limits in computation of $\mathcal{L}_{\mathcal{I}_{\mathcal{M}}}$ in (A.3) are from x_M to ∞, as the nearest co-tier interferer must be at least farther than x_M. Simplifying the integrand in (A.3) by substituting $u_M = (x_M^{\alpha_{1M}}\tau)^{-2/\alpha_{1M}}y^2$ and solving it gives

$$\mathcal{L}_{\mathcal{I}_{\mathcal{M}}}\left(\frac{\tau\, x_M^{\alpha_{1M}}}{P_M\eta_M}\right) = \exp\left(\frac{-2\pi\lambda_M\tau x_M^2}{N(-2+\alpha_{1M})}{}_2F_1\left[1, 1-\frac{2}{\alpha_{1M}}; 2-\frac{2}{\alpha_{1M}}; -\tau\right]\right), \tag{A.4}$$

where ${}_2F_1[.]$ is the well-known Gauss Hypergeometric function and (A.4) gives the contribution of macro tier interference in CCDF conditioned on x_M greater than R_{CM}. Similar to (A.3), the $\mathcal{L}_{\mathcal{I}_{\mathcal{S}}}$ is also expressed as

$$\mathcal{L}_{\mathcal{I}_{\mathcal{S}}}\left(\frac{\tau\, x_M^{\alpha_{1M}}}{P_M\eta_M}\right) = e^{\frac{-2\pi\lambda_S}{N}\begin{cases}\int_{g_0(x_M)}^{\infty}\frac{y}{1+\left(x_M^{\alpha_{1M}}\frac{P_S}{P_M\eta_M}\tau\right)^{-1}y^{\alpha_{0S}}}\mathrm{d}y & g_1(x_M) \le R_{CS}\\ \int_{g_1(x_M)}^{\infty}\frac{y}{1+\left(x_M^{\alpha_{1M}}\frac{P_S\eta_S}{P_M\eta_M}\tau\right)^{-1}y^{\alpha_{1S}}}\mathrm{d}y & g_1(x_M) > R_{CS}\end{cases}}. \tag{A.5}$$

It is clear from (A.5), that computing the received interference from neighboring SBSs requires solving two integrals. This is because, the T-UE may associate with macro tier both within and outside R_{CS} while its distance from nearest MBS i.e., x_M is greater than R_{CM}. The received interference from within R_{CS} is determined with integration limits $g_0(x_M)$ to ∞ while the limits for the second integral are from $g_1(x_M)$ to ∞. Moreover, similar to (A.3), the T-UE receives interference from only those SBSs which are operating at the frequency of its associated MBS.

Now, simplifying the integrands in (A.5) by using suitable substitutions gives

$$\mathcal{L}_{\mathcal{I}_S}\left(\frac{\tau\, x_M^{\alpha_{1M}}}{P_M\eta_M}\right)=\begin{cases}\exp\left(\dfrac{-2\pi\lambda_S\tau(g_1(x_M))^2}{N(-2+\alpha_{1S})}\right.\\ \left.\times\ {}_2F_1\left[1,1-\dfrac{2}{\alpha_{1S}};2-\dfrac{2}{\alpha_{1S}};-\dfrac{\tau}{B_S}\right]\right)\\ \qquad\qquad g_1(x_M)\geq R_{CS}\\ \exp\left(\dfrac{-2\pi\lambda_S}{N}\left(\dfrac{(g_0(x_M))^2}{2}\right.\right.\\ \times\ {}_2F_1\left[1,\dfrac{2}{\alpha_{0S}};1+\dfrac{2}{\alpha_{0S}};-\dfrac{B_S}{\tau}\right]+\dfrac{R_{CS}^2}{2}\\ \times\ {}_2F_1\left[1,\dfrac{2}{\alpha_{0S}};1+\dfrac{2}{\alpha_{0S}};-c_2(x_M)\right]\\ +\dfrac{P_S\eta_S\tau\, x_M^{\alpha_{1M}}}{P_M\eta_M(-2+\alpha_{1S})}\left(R_{CS}^{2-\alpha_{1S}}\right)\\ \left.\left.\times\ {}_2F_1\left[1,1-\dfrac{2}{\alpha_{1S}};2-\dfrac{2}{\alpha_{1S}};-c_3(x_M)\right]\right)\right)\\ \qquad\qquad g_1(x_M)<R_{CS}\end{cases},\tag{A.6}$$

where, $c_2(x_M)=(P_M\eta_M(R_{CS})^{\alpha_{0S}})/(P_S\tau(x_M)^{\alpha_{1M}})$ and $c_3(x_M)=(P_S\eta_S\tau(x_M)^{\alpha_{1M}})/(P_M\eta_M(R_{CS})^{\alpha_{1S}})$, while (A.6) gives the contribution of inter-tier interference in macro CCDF conditioned on x_M greater than R_{CM}. Now by plugging the respective values of $\mathcal{L}_{\mathcal{I}_M}$ and $\mathcal{L}_{\mathcal{I}_S}$ in (A.1), completes the proof of (30).

References

[1] Ericsson, Ericsson mobility report June 2019, 2019, [Online]. Available: https://www.ericsson.com/en/mobility-report reports/june-2019.

[2] M. Patzold, 5G Is going live in country after country [mobile radio], IEEE Veh. Tech. Mag. 14 (4) (2019) 4–10, https://doi.org/10.1109/mvt.2019.2939756.

[3] A. Damnjanovic, J. Montojo, Y. Wei, T. Ji, T. Luo, M. Vajapeyam, T. Yoo, O. Song, D. Malladi, A survey on 3GPP heterogeneous networks, IEEE Wireless Commun. 18 (3) (2011) 10–21, https://doi.org/10.1109/mwc.2011.5876496.

[4] J.G. Andrews, Seven ways that hetnets are a cellular paradigm shift, IEEE Commun. Mag. 51 (3) (2013) 136–144, https://doi.org/10.1109/mcom.2013.6476878.

[5] Q.C. Li, H. Niu, A.T. Papathanassiou, G. Wu, 5G Network capacity: key elements and technologies, IEEE Veh. Technol. Mag. 9 (1) (2014) 71–78, https://doi.org/10.1109/mvt.2013.2295070.

[6] S. Mollahasani, A. Eroğlu, I. Demirkol, E. Onur, Density-aware mobile networks: opportunities and challenges, Comput. Netw. 175 (2020) 107271, https://doi.org/10.1016/j.comnet.2020.107271.

[7] J.G. Andrews, F. Baccelli, R.K. Ganti, A tractable approach to coverage and rate in cellular networks, IEEE Trans. Commun. 59 (11) (2011) 3122–3134, https://doi.org/10.1109/tcomm.2011.100411.100541.

[8] H.S. Dhillon, R.K. Ganti, F. Baccelli, J.G. Andrews, Modeling and analysis of K-tier downlink heterogeneous cellular networks, IEEE J. Sel. Areas Commun. 30 (3) (2012) 550–560, https://doi.org/10.1109/jsac.2012.120405.

[9] X. Ge, Y. Qiu, J. Chen, M. Huang, H. Xu, J. Xu, W. Zhang, Y. Yang, C.-X. Wang, J. Thompson, Wireless fractal cellular networks, IEEE Wireless Commun. 23 (5) (2016) 110–119, https://doi.org/10.1109/mwc.2016.7721749.

[10] Y. Hao, M. Chen, L. Hu, J. Song, M. Volk, I. Humar, Wireless fractal ultra-dense cellular networks, Sensors 17 (4) (2017) 841, https://doi.org/10.3390/s17040841.

[11] J. Chen, X. Ge, Q. Ni, Coverage and handoff analysis of 5G fractal small cell networks, IEEE Trans. Wirel. Commun. 18 (2) (2019) 1263–1276, https://doi.org/10.1109/twc.2018.2890662.

[12] D. López-Pérez, M. Ding, H. Claussen, A.H. Jafari, Towards 1 gbps/ue in cellular systems: understanding ultra-dense small cell deployments, IEEE Commun. Surv. Tutor. 17 (4) (2015) 2078–2101, https://doi.org/10.1109/comst.2015.2439636.

[13] K. Son, S. Lee, Y. Yi, S. Chong, Refim: a practical interference management in heterogeneous wireless access networks, IEEE J. Sel. Areas Commun. 29 (6) (2011) 1260–1272, https://doi.org/10.1109/jsac.2011.110613.

[14] N. Saquib, E. Hossain, L.B. Le, D.I. Kim, Interference management in ofdma femtocell networks: issues and approaches, IEEE Wirel. Commun. 19 (3) (2012) 86–95, https://doi.org/10.1109/mwc.2012.6231163.

[15] T.D. Novlan, R.K. Ganti, A. Ghosh, J.G. Andrews, Analytical evaluation of fractional frequency reuse for heterogeneous cellular networks, IEEE Trans. Commun. 60 (7) (2012) 2029–2039, https://doi.org/10.1109/tcomm.2012.061112.110477.

[16] E. Hossain, M. Rasti, H. Tabassum, A. Abdelnasser, Evolution toward 5G multi-tier cellular wireless networks: an interference management perspective, IEEE Wirel. Commun. 21 (3) (2014) 118–127, https://doi.org/10.1109/mwc.2014.6845056.

[17] A. Mukherjee, D. De, P. Deb, Interference management in macro-femtocell and micro-femtocell cluster-based long-term evaluation-advanced green mobile network, IET Commun. 10 (5) (2016) 468–478, https://doi.org/10.1049/iet-com.2015.0982.

[18] N. Hassan, X. Fernando, Interference mitigation and dynamic user association for load balancing in heterogeneous networks, IEEE Trans. Veh. Tech. 68 (8) (2019) 7578–7592, https://doi.org/10.1109/tvt.2019.2919812.

[19] S. Singh, H.S. Dhillon, J.G. Andrews, Offloading in heterogeneous networks: modeling, analysis, and design insights, IEEE Trans. Wirel. Commun. 12 (5) (2013) 2484–2497, https://doi.org/10.1109/twc.2013.040413.121174.

[20] Q. Ye, B. Rong, Y. Chen, M. Al-Shalash, C. Caramanis, J.G. Andrews, User association for load balancing in heterogeneous cellular networks, IEEE Trans. Wirel. Commun. 12 (6) (2013) 2706–2716, https://doi.org/10.1109/twc.2013.040413.120676.

[21] X. Ge, X. Li, H. Jin, J. Cheng, V.C. Leung, Joint user association and user scheduling for load balancing in heterogeneous networks, IEEE Trans. Wirel. Commun. 17 (5) (2018) 3211–3225, https://doi.org/10.1109/twc.2018.2808488.

[22] A. Shaverdian, J. Ghimire, C. Rosenberg, Simple and efficient network-aware user association rules for heterogeneous networks, Comput. Netw. 156 (2019) 20–32, https://doi.org/10.1016/j.comnet.2019.04.001.

[23] M. Zalghout, A. Khalil, M. Crussiére, S. Abdul-Nabi, J.F. Hélard, Context-aware and priority-based user association and resource allocation in heterogeneous wireless networks, Comput. Netw. 149 (2019) 76–92.

[24] M. Fereydooni, M. Sabaei, M. Dehghan, G.B. Eslamlou, M. Rupp, Analytical evaluation of heterogeneous cellular networks under flexible user association and frequency reuse, Comput. Commun. 116 (2018) 147–158, https://doi.org/10.1016/j.comcom.2017.11.014.

[25] H.-S. Jo, Y.J. Sang, P. Xia, J.G. Andrews, Heterogeneous cellular networks with flexible cell association: a comprehensive downlink SINR analysis, IEEE Trans. Wirel. Commun. 11 (10) (2012) 3484–3495, https://doi.org/10.1109/twc.2012.081612.111361.

[26] S. Lee, K. Huang, Coverage and economy of cellular networks with many base stations, IEEE Commun. Lett. 16 (7) (2012) 1038–1040, https://doi.org/10.1109/lcomm.2012.042512.120426.

[27] H.S. Dhillon, R.K. Ganti, J.G. Andrews, Load-aware modeling and analysis of heterogeneous cellular networks, IEEE Trans. on Wirel. Commun. 12 (4) (2013) 1666–1677, https://doi.org/10.1109/twc.2013.13.120485.

[28] P.D. Mankar, G. Das, S.S. Pathak, Load-aware performance analysis of cell center/edge users in random hetnets, IEEE Trans. Veh. Tech. 67 (3) (2017) 2476–2490, https://doi.org/10.1109/tvt.2017.2681158.

[29] M. Ding, D. López-Pérez, G. Mao, Z. Lin, Performance impact of idle mode capability on dense small cell networks, IEEE Trans. Veh. Tech. 66 (11) (2017) 10446–10460, https://doi.org/10.1109/tvt.2017.2754416.

[30] C. Galiotto, N.K. Pratas, L. Doyle, N. Marchetti, Effect of LOS/NLOS propagation on 5g ultra-dense networks, Comput. Networks 120 (2017) 126–140, https://doi.org/10.1016/j.comnet.2017.04.012.

[31] H. ElSawy, E. Hossain, M. Haenggi, Stochastic geometry for modeling, analysis, and design of multi-tier and cognitive cellular wireless networks: a survey, IEEE Commun. Surv. Tutor. 15 (3) (2013) 996–1019, https://doi.org/10.1109/SURV.2013.052213.00000.

[32] A. Ullah, Z.H. Abbas, G. Abbas, F. Muhammad, L. Jiao, Performance analysis of user-centric sbs deployment with load balancing in heterogeneous cellular networks: a thomas cluster process approach, Comput. Netw. (2020) 107–120, https://doi.org/10.1016/j.comnet.2020.107120.

[33] A.V. Savkin, H. Huang, Deployment of unmanned aerial vehicle base stations for optimal quality of coverage, IEEE Wireless Commun. Lett. 8 (1) (2018) 321–324, https://doi.org/10.1109/lwc.2018.2872547.
[34] H. Huang, A.V. Savkin, A method for optimized deployment of unmanned aerial vehicles for maximum coverage and minimum interference in cellular networks, IEEE Trans. Ind. Inform. 15 (5) (2018) 2638–2647, https://doi.org/10.1109/tii.2018.2875041.
[35] Y. Zeng, R. Zhang, T.J. Lim, Wireless communications with unmanned aerial vehicles: opportunities and challenges, IEEE Commun. Mag. 54 (5) (2016) 36–42, https://doi.org/10.1109/mcom.2016.7470933.
[36] B. Li, Z. Fei, Y. Zhang, UAV Communications for 5g and beyond: recent advances and future trends, IEEE Internet Things J. 6 (2) (2018) 2241–2263, https://doi.org/10.1109/jiot.2018.2887086.
[37] M. Mozaffari, A.T.Z. Kasgari, W. Saad, M. Bennis, M. Debbah, Beyond 5G with UAVs: foundations of a 3D wireless cellular network, IEEE Trans. on Wirel. Commun. 18 (1) (2018) 357–372, https://doi.org/10.1109/twc.2018.2879940.
[38] H. Wang, X. Zhou, M.C. Reed, Coverage and throughput analysis with a non-uniform small cell deployment, IEEE Trans. Wirel. Commun. 13 (4) (2014) 2047–2059, https://doi.org/10.1109/TWC.2014.022014.130855.
[39] F. Muhammad, Z.H. Abbas, F.Y. Li, Cell association with load balancing in nonuniform heterogeneous cellular networks: coverage probability and rate analysis, IEEE Trans. Veh. Techn. 66 (6) (2016) 5241–5255, https://doi.org/10.1109/TVT.2016.2614696.
[40] Z.H. Abbas, F. Muhammad, L. Jiao, Analysis of load balancing and interference management in heterogeneous cellular networks, IEEE Access 5 (2017) 14690–14705, https://doi.org/10.1109/ACCESS.2017.2732498.
[41] M.S. Haroon, Z.H. Abbas, G. Abbas, F. Muhammad, Coverage analysis of ultra-dense heterogeneous cellular networks with interference management, Wirel. Netw. (2020) 2013–2025, https://doi.org/10.1007/s11276-019-01965-0.
[42] N. Deng, W. Zhou, M. Haenggi, Heterogeneous cellular network models with dependence, IEEE J. Sel. Areas Commun. 33 (10) (2015) 2167–2181, https://doi.org/10.1109/JSAC.2015.2435471.
[43] R. Hernandez-Aquino, S.A.R. Zaidi, M. Ghogho, D. McLernon, A. Swami, Stochastic geometric modeling and analysis of non-uniform two-tier networks: a Stienen's model-based approach, IEEE Trans. Wirel. Commun. 16 (6) (2017) 3476–3491, https://doi.org/10.1109/TWC.2017.2682844.
[44] M.S. Haroon, Z.H. Abbas, F. Muhammad, G. Abbas, Analysis of coverage-oriented small base station deployment in heterogeneous cellular networks, Phys. Commun. 38 (2020) 100908, https://doi.org/10.1016/j.phycom.2019.100908.
[45] M.S. Haroon, Z.H. Abbas, F. Muhammad, G. Abbas, Coverage analysis of cell-edge users in heterogeneous wireless networks using Stienen's model and RFA scheme, Int. J. Commun. Syst. (2019) e4147, https://doi.org/10.1002/dac.4147.
[46] Z. Zhang, R.Q. Hu, Dense cellular network analysis with LoS/NLospropagation and bounded path loss model, IEEE Commun. Lett. 22 (11) (2018) 2386–2389, https://doi.org/10.1109/lcomm.2018.2850815.
[47] I. Atzeni, J. Arnau, M. Kountouris, Downlink cellular network analysis with LOS/NLOS propagation and elevated base stations, IEEE Trans. Wirel. Commun. 17 (1) (2018) 142–156, https://doi.org/10.1109/twc.2017.2763136.
[48] M. Ding, P. Wang, D. López-Pérez, G. Mao, Z. Lin, Performance impact of LoS and NLoS transmissions in dense cellular networks, IEEE Trans. Commun. 15 (3) (2015) 2365–2380, https://doi.org/10.1109/twc.2015.2503391.
[49] M. Ding, D. López-Pérez, On the performance of practical ultra-dense networks: The major and minor factors. 2017 15th International Symposium on Modeling and Optimization in Mobile, Ad Hoc, and Wireless Networks (WiOpt), IEEE, 2017, pp. 1–8.Doi:10.23919/wiopt.2017.7959926
[50] X. Zhang, J.G. Andrews, Downlink cellular network analysis with multi-slope path loss models, IEEE Trans. Commun. 63 (5) (2015) 1881–1894, https://doi.org/10.1109/tcomm.2015.2413412.
[51] H. Munir, S.A. Hassan, H. Pervaiz, Q. Ni, L. Musavian, Resource optimization in multi-tier hetnets exploiting multi-slope path loss model, IEEE Access 5 (2017) 8714–8726, https://doi.org/10.1109/access.2017.2699941.
[52] M.J. Feuerstein, K.L. Blackard, T.S. Rappaport, S.Y. Seidel, H.H. Xia, Path loss, delay spread, and outage models as functions of antenna height for microcellular system design, IEEE Trans. Veh. Tech. 43 (3) (1994) 487–498, https://doi.org/10.1109/25.312809.
[53] K. Shehzad, N.M. Khan, J. Ahmed, Impact of frequency reuse and flexible cell association on the performance of dense heterogeneous cellular networks using dual-slope path loss model, IEEE Access 7 (2019) 166214–166234, https://doi.org/10.1109/access.2019.2952915.
[54] S.N. Chiu, D. Stoyan, W.S. Kendall, J. Mecke, Stochastic Geometry and its Applications, John Wiley & Sons, 2013.Doi:10.1002/9781118658222
[55] B. Błaszczyszyn, M.K. Karray, H.P. Keeler, Wireless networks appear poissonian due to strong shadowing, IEEE Trans. Wirel. Commun. 14 (8) (2015) 4379–4390, https://doi.org/10.1109/twc.2015.2420099.
[56] M. Haenggi, On distances in uniformly random networks, IEEE Trans. Inf. Theory 51 (10) (2005) 3584–3586, https://doi.org/10.1109/tit.2005.855610.

Khurram Shehzad received his Bachelor degree in Electrical Engineering from COMSATS Institute of Information and Technology (CIIT), Islamabad, Pakistan in 2009 and M.S. degree in Computer Engineering from UET Taxila, Pakistan in 2012. Presently, he is pursuing his Ph.D. from Capital University of Science and Technology, Islamabad, Pakistan. His research interests include modeling of heterogeneous cellular networks, communication theory, and applications of stochastic geometry in wireless networks.

Noor Muhammad Khan received the B.Sc. degree in electrical engineering from UET Lahore in 1998. He held several positions in World Call Communications, National Institute of Science and Technical Education (NISTE), and Pakistan Telecommunication Company Limited (PTCL) from 1999 to 2002. In 2002, he joined the school of electrical and telecommunications, University of New South Wale (UNSW), Sydney Australia, where he completed his Ph.D. degree in electrical engineering in March 2006. Currently, he is working as a Professor and head of Acme Center for Research in Wireless Communications (ARWiC) at Capital University of Science and Technology, Islamabad, Pakistan. His research interests include smart antenna system, wireless sensor networks, channel modeling, adaptive multiuser detection and mobile to mobile communication systems.

Junaid Ahmed received his PhD degree from The University of Manchester, UK in 2011. Since June 2004 he is with the Department of Electrical Engineering at COMSATS University Islamabad, Pakistan, where he serves as an Assistant Professor. His research interests include heterogeneous networks, D2D and V2X communication and interference management in 5G cellular networks.